The interplay between active hair bundle motility and electromotility in the cochlea

Dáibhid Ó Maoiléidigh and Frank Jülicher[a)]
Max Planck Institute for the Physics of Complex Systems, Nöthnitzer Straße 38, 01187 Dresden, Germany

(Received 5 February 2010; revised 15 June 2010; accepted 16 June 2010)

The cochlear amplifier is a nonlinear active process providing the mammalian ear with its extraordinary sensitivity, large dynamic range and sharp frequency tuning. While there is much evidence that amplification results from active force generation by mechanosensory hair cells, there is debate about the cellular processes behind nonlinear amplification. Outer hair cell electromotility has been suggested to underlie the cochlear amplifier. However, it has been shown in frog and turtle that spontaneous movements of hair bundles endow them with a nonlinear response with increased sensitivity that could be the basis of amplification. The present work shows that the properties of the cochlear amplifier could be understood as resulting from the combination of both hair bundle motility and electromotility in an integrated system that couples these processes through the geometric arrangement of hair cells embedded in the cochlear partition. In this scenario, the cochlear partition can become a dynamic oscillator which in the vicinity of a Hopf bifurcation exhibits all the key properties of the cochlear amplifier. The oscillatory behavior and the nonlinearity are provided by active hair bundles. Electromotility is largely linear but produces an additional feedback that allows hair bundle movements to couple to basilar membrane vibrations.
 [DOI: 10.1121/1.3463804]

PACS number(s): 43.64.Kc, 43.64.Bt, 43.64.Ld [BLM] Pages: 1175–1190

I. INTRODUCTION

The extraordinary ability of the vertebrate ear to detect sound stimuli relies on an active process which amplifies weak stimuli and which permits the ear to operate over a vast range of sound amplitude.[1,2] Four key signatures have been associated with this active process.[1,3] (i) A high sensitivity to weak signals,[4,5] (ii) a compressive nonlinear response as a function of signal amplitude,[4–6] (iii) sharp frequency tuning[6,7] and (iv) the existence of spontaneous otoacoustic emissions.[8,9] All of these signatures are physiologically vulnerable and have been linked to cellular processes.[4,5,7,10,11] It has been suggested that these signatures are the consequence of sets of dynamic oscillators acting in the hearing organs of vertebrates to serve as nonlinear amplifiers, each operating close to an oscillating instability or Hopf bifurcation and tuned to a specific frequency.[12–15] While this general principle can account for the basic properties of the active process, the precise nature of the active processes in vertebrate hearing organs have remained a matter of debate and controversy. There is a lot of evidence that the mechanosensory hair cells of the ear exhibit active behaviors that generate the auditory amplifier.[1,2,16–20] Two mechanisms have been suggested to underlie the active process in mammals: outer hair cell electromotility and active hair bundle motility.

The discovery of the electromotility of mammalian outer hair cells[21–23] has stimulated many studies to elucidate the role of this electro-mechanical coupling in the cochlear amplifier.[24] Electromotility is the ability of outer hair cells to change their length upon a change in membrane potential. Interestingly, the piezoelectric coefficient which characterizes electromotility is over four orders of magnitude larger than that of any other material.[25] It has been suggested that outer hair cell electromotility provides a positive feedback that reduces viscous damping in the ear and contributes to active amplification.[2,18,26,27] However, outer hair cell electromotility alone is not significantly nonlinear within the physiological range of receptor potential changes.[28,29] Furthermore, a direct demonstration that electromotility can generate spontaneous oscillations is lacking.

Another important property of hair cells that could be involved in auditory amplification is the ability of hair bundles to generate spontaneous movements and forces.[30–33] Hair bundles are the mechanosensory organelles of hair cells. They are formed by groups of stiff, actin based stereocilia which are linked by tiny filaments, so-called tip links that are involved in the gating of transduction channels. Deflection of the stereocilia triggers the opening of these channels. The resulting ion flux generates a change in hair cell membrane potential. Myosin motors mediate adaptation of the transduction machinery.[16] Interestingly, hair bundles in turtle and frog have been shown to exhibit spontaneous oscillations.[30–32] The frequency of the observed oscillations range from a few Hertz to over a hundred Hertz.[32,34] These oscillations endow the hair bundle with nonlinear amplification and three of the signatures of the cochlear amplifier have been observed in active hair bundles.[31,35] However, individual hair bundles are only modest amplifiers with an amplification gain (ratio of maximum sensitivity to minimum sensitivity) that is limited by fluctuations to about 10, much smaller than the observed amplification in the mammalian cochlea of up to 1000.[5,35] In

a)Author to whom correspondence should be addressed. Electronic mail: julicher@pks.mpg.de

mammals it has been shown that the hair bundle is active and has a nonlinear response in the cochlea, but spontaneous oscillations have so far not been reported.[33,36]

The role of electromotility and active hair bundle motility in the cochlear amplifier and its compressive nonlinearity remain a matter of debate. Genetic mutants, where the electromotile properties of the outer hair cell are reduced or lacking, show that outer hair cell electromotility is required for the function of the amplifier.[37,38] However, there are conceptual difficulties associated with electromotility mediated amplification. For example, it has been remarked that although the electromotile response is fast enough to function at high frequencies[39] it may not work effectively due to the low pass filtering of the transmembrane receptor potential by the basolateral membrane capacitance and resistance.[28,40] This is known as the RC time constant problem as this low pass filtering may be described by a simple RC circuit. Solutions to this problem have been suggested,[24,41–43] but experimental verification is lacking. The performance of hair bundles on the other hand may be strongly limited by fluctuations, although it is possible that collections of hair bundles coupled by the tectorial membrane may respond synchronously to enhance the amplificatory properties of the group.[44] Nonetheless, it has been questioned if hair bundles are positioned in the cochlea such as to generate significant basilar membrane displacements and thus drive the cochlear amplifier.[45]

The cochlea of the mammalian inner ear is a long fluid filled chamber where sound stimulation is converted into an electrical signal for transmission to the brain by the auditory nerve.[2,18,46] This chamber is bisected by the cochlear partition, housing the sensory hair cells. Acoustic stimulation results in a wave which travels along the partition and peaks at a frequency dependent position which is determined by the local properties of the partition. The cochlear traveling wave is boosted in the proximity of this characteristic place by the cochlear amplifier located in the partition.[2,18,27] The sound induced deformations of the cochlear partition result in the deflection of the hair bundles of the sensory hair cells.

Many descriptions of cochlear mechanics have been proposed ranging from passive models[45,47–49] to active ones.[50–54] In active models the activity is often introduced as a negative damping element[50,51] or by associating an active force with outer hair cells.[52,53] Moreover, particular phase relationships between the components of the partition are often hypothesized.[52–54] In principle, it is possible to derive the coupling between the outer hair cell electromotile force and partition displacements from the observed geometrical and viscoelastic properties of the cochlea.

Here we develop a theoretical description of the auditory amplifier in the cochlear partition which combines outer hair cell electromotility with active hair bundle motility. We consider a slice through the cochlea at some longitudinal position and analyze the interplay between the passive and active mechanical properties of the hair cells and the other structural elements as well as the outer hair cell membrane potential. We show that the combination of hair bundle motility and electromotility of outer hair cells results in a dynamic oscillatory module that can be controlled to operate in the vicinity of a Hopf bifurcation. This integrated system exhibits many of the features of the auditory amplifier of the mammalian cochlea. In this picture, the active process is driven by the activity of myosin adaptation motors in the hair bundle as well as electrochemical gradients across the outer hair cell membrane.

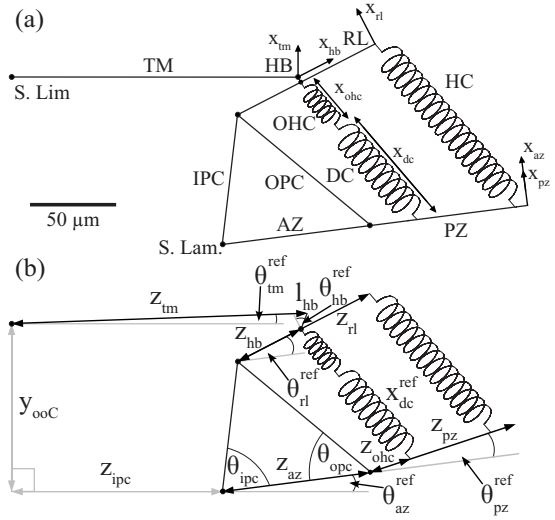

FIG. 1. Simplified model of the cochlear partition. We represent some structural elements by rigid beams, and others as elastic springs. (a) Rigid elements are: TM–tectorial membrane, HB–hair bundle, RL–reticular lamina, AZ–arcuate zone of the basilar membrane, PZ–pectinate zone of the basilar membrane, IPC–inner pillar cell and OPC–outer pillar cell. The following structures are represented by elastic springs: OHC–outer hair cells, DC–Deiters' cells and HC–Hensen's cells. The circles indicate pivot points. The positions of two pivot points are fixed: S. Lim.–the point where the TM meets the spiral limbus, S. Lam.–point where the basilar membrane meets the spiral lamina. The relevant displacement variables are indicated by arrows. (b) Geometric parameters for the cochlear partition. The geometric parameters describing the cochlear partition are defined here with parameter values given in Table IV. The parameters corresponding to fixed lengths are: z_{tm}–length of the TM connection between the HB and the S. Lim., z_{hb}–distance between the apex of Corti's arches and the HB, z_{rl}–length of the RL from the apex of Corti's arches to the HC, z_{ipc}–radial distance between the S. Lim. and the S. Lam., z_{az}–length of the AZ, z_{ohc}–distance between the base of the OPC and the base of the DC, z_{pz}–half the length of the PZ, l_{hb}–length of the HB and y_{ooC}–vertical distance between the S. Lim. and the S. Lam. The parameters corresponding to fixed angles are: θ_{ipc}–the angle between the IPC and the AZ and θ_{opc}–the angle between the OPC cell and the AZ. The length of the DC is x_{dc}^{ref} in the reference state. The rigid beam angles in the reference state are: θ_{tm}^{ref}–the angle between the TM beam and the horizontal, θ_{hb}^{ref}–the angle between the HB and the RL perpendicular, θ_{az}^{ref}–the angle between the AZ and the horizontal, θ_{pz}^{ref}–the angle between the PZ and the AZ and θ_{rl}^{ref}–the angle between the RL and the AZ.

II. COCHLEAR MECHANICS AND HAIR CELL DYNAMICS

We present a physical description of the mechanics of the cochlear partition which takes into account outer hair cell mechanics, electromotility, ion current dynamics as well as hair bundle mechanics. We obtain the dynamical equations starting from the known geometry of the partition and from known properties of outer hair cells embedded in the partition.

A. Cochlear geometry and micromechanics

The mechanics of a passive slice of the cochlear partition containing one row of outer hair cells is described as a

system of springs attached to rigid beams, which may pivot about their ends (Fig. 1). For simplicity, we represent the three outer hair cells in this slice by one effective outer hair cell element. Our description is based on the cochlear structure and observed deformations during stimulation.[55–62] We define the deformation relative to a resting reference state corresponding to a quiescent cochlea using the set of variables shown in Fig. 1. These variables are the deflections of the tectorial membrane x_{tm}, the reticular lamina x_{rl} and of the hair bundle x_{hb}. We describe basilar membrane deflections with two independent variables, x_{az} and x_{pz}, corresponding to deformations of the arcuate and the pectinate zones, respectively. In addition, we introduce the change in length of the outer hair cells x_{ohc}, of the Deiters' cells x_{dc} and of Hensen's cells x_{hc}. Geometric constraints due to the rigid beam elements in Fig. 1 imply that deformation variables cannot vary independently. We choose to express these constraints such that the variables x_{tm}, x_{rl}, x_{dc} and x_{hc} are determined from the values of x_{hb}, x_{ohc}, x_{az} and x_{pz}. These relations are nonlinear and follow from the geometry depicted in Fig. 1 (see Appendix A). For the small angular changes that result from sound stimuli in the physiological range, nonlinearities are unimportant and a linearized version of these constraints is sufficient. In this linearized regime, the constraints can be written as

$$\begin{pmatrix} x_{tm} \\ x_{rl} \\ x_{dc} \\ x_{hc} \end{pmatrix} = \mathbf{\Gamma} \cdot \begin{pmatrix} x_{hb} \\ x_{ohc} \\ x_{az} \\ x_{pz} \end{pmatrix}, \tag{1}$$

where $\mathbf{\Gamma}$ is a matrix of dimensionless coefficients describing the geometry of the cochlear partition. This matrix has the form

$$\mathbf{\Gamma} = \begin{pmatrix} \gamma_{11} & 0 & \gamma_{13} & 0 \\ \gamma_{21} & 0 & \gamma_{23} & 0 \\ \gamma_{31} & -1 & \gamma_{33} & \gamma_{34} \\ \gamma_{41} & 0 & \gamma_{43} & \gamma_{44} \end{pmatrix}. \tag{2}$$

Several matrix elements vanish because of independence between certain variables and one entry is $\gamma_{32}=-1$, reflecting the geometric relation between outer hair cells and Deiters' cells. For the system shown in Fig. 1, we express force balances involving inertial forces, friction forces, forces due to elastic elements as well as the externally applied force exerted through the pressure difference P_{ext}, acting on the partition. Using the constraints described above, this force balance can be expressed as (see Appendix A)

$$\begin{pmatrix} m_1\ddot{x}_{hb} - m_2\ddot{x}_{az} + \lambda\dot{x}_{hb} \\ \lambda_{ohc}\dot{x}_{ohc} \\ m_{az}\ddot{x}_{az} - m_2\ddot{x}_{hb} + \lambda_{az}\dot{x}_{az} \\ m_{pz}\ddot{x}_{pz} + \lambda_{pz}\dot{x}_{pz} \end{pmatrix} = \boldsymbol{K} \cdot \begin{pmatrix} x_{hb} \\ x_{ohc} \\ x_{az} \\ x_{pz} \end{pmatrix} + \begin{pmatrix} 0 \\ 0 \\ \mu_{az} \\ \mu_{pz} \end{pmatrix} P_{ext}. \tag{3}$$

The left hand side of this equation describes inertial and friction forces, where m_{az}, m_{pz}, m_1 and m_2 denote masses, and λ, λ_{ohc}, λ_{az} and λ_{pz} are friction coefficients. In deriving these equations, we have introduced the inertia of the basilar membrane and the tectorial membrane. The geometric constraints generate the inertial terms m_1, m_2, which depend upon the tectorial membrane mass. The term m_{az} depends on both the tectorial membrane mass and the basilar membrane mass. The effects of elastic elements in the cochlear partition are described by the symmetric matrix

$$\boldsymbol{K} = \begin{pmatrix} -K_{11} & K_{12} & K_{13} & K_{14} \\ K_{12} & -K_{22} & -K_{23} & -K_{24} \\ K_{13} & -K_{23} & -K_{33} & -K_{34} \\ K_{14} & -K_{24} & -K_{34} & -K_{44} \end{pmatrix} \tag{4}$$

of elastic coefficients. Furthermore, the coefficients μ_{az} and μ_{pz} are the effective areas relating the pressure P_{ext} to the forces that act on the cochlear partition. The force balance [Eq. (3)] describes the passive dynamics of the model shown in Fig. 1, taking into account geometric constraints, elastic elements, inertia and friction. For simplicity, we only include friction coefficients associated with the variables x_{hb}, x_{ohc}, x_{az} and x_{pz}. These friction coefficients include contributions from the variables x_{tm}, x_{rl}, x_{dc} and x_{hc} due to the constraints of Eq. (1). In particular, λ includes contributions from the hair bundle, the fluid in the subtectorial space, the tectorial membrane, the reticular lamina, Deiters' cells and Hensen's cells and can be much larger than the friction coefficient associated with an isolated hair bundle. More generally, friction could also couple different variables, an effect we neglect here. The coefficients of the matrices Γ and K defined in Eq. (2) and Eq. (4) are calculated explicitly in terms of the geometric and elastic properties of the cochlear partition.

B. Hair bundle mechanics

We describe the dynamics and mechanics of the hair bundle with two degrees of freedom: the deflection of the hair bundle x_{hb}, and the displacement of myosin adaptation motors x_a. These variables obey the equations[32,63,64]

$$\lambda_{hb}\dot{x}_{hb} = -K_{gs}(x_{hb} - x_a - DP_o) - K_{sp}x_{hb} + f_{ext}, \tag{5}$$

$$\lambda_a\dot{x}_a = K_{gs}(x_{hb} - x_a - DP_o) - \gamma f_{max}(1 - SP_o). \tag{6}$$

Equation (5) describes the force balance for the hair bundle subject to an external force f_{ext}. The dynamics of adaptation motors given by Eq. (6) is based on a linear force-velocity relation. Here f_{max} is the maximum force the motors can produce, λ_{hb} and λ_a are damping coefficients, and K_{gs} and K_{sp} are the stiffnesses of gating springs and of the stereociliary pivots, respectively. The hair bundle displacement associated with transduction channel opening is denoted by D, γ is a dimensionless geometric factor and S is a dimensionless measure of the strength of the calcium feedback which controls motor activity. Finally, P_o is the open probability of the transduction channels

$$P_o(x_{hb}-x_a)=\left(1+A\,\exp\left(-\frac{(x_{hb}-x_a)}{\delta_{hb}}\right)\right)^{-1}, \tag{7}$$

where $1/(1+A)$ is the open probability when the gating springs are severed and δ_{hb} is a characteristic distance over which channels open.

It has been shown previously that this model can describe active hair bundle motility observed in different systems including frog, turtle and rat.[63,64] The hair bundle model given by Eq. (5) and Eq. (6) is characterized by a state diagram as a function of the control parameters f_{max} and S. There exists a region of this state diagram where the hair bundle oscillates spontaneously.[63]

C. Outer hair cell electromotility and ion currents

Outer hair cell electromotility is described as a linear piezoelectric system which couples mechanics to membrane potential

$$F=-K_{ohc}x_{ohc}-pQ, \tag{8}$$

$$V=px_{ohc}+\frac{Q}{C_{ohc}}. \tag{9}$$

Here F is the variation of the mechanical force exerted by the outer hair cells, V is the change of the membrane potential and Q is the charge displaced across the outer hair cells' membranes. The length change x_{ohc} of the outer hair cells has been introduced in Section II A. The stiffness of these outer hair cells is denoted $K_{ohc}=K_{22}$, C_{ohc} is the capacitance of the outer hair cells' membranes and p is the piezoelectric coefficient describing the electromotile response.

The current flow through the outer hair cells involves several ion types.[40,65] For simplicity we describe the flow of charge through the outer hair cells with a single effective ion species of positive charge as most of the current through the outer hair cell is carried by potassium.[65] We consider the scala media and scala tympani to be large reservoirs of ions where the ion concentrations are approximately constant. In other words, we assume that the endocochlear potential is approximately constant so that the changes in the electrochemical gradients across the outer hair cell membranes are given by the change in the outer hair cell electrochemical potential. In general, the current from outside to inside the outer hair cell $\dot{Q}$, is a function of the open probability of the mechanoelectrical ion channels P_o, the electric potential of the interior of the outer hair cell V_{ohc}, and the intracellular concentration of the effective ion species $[\kappa_{ohc}]$. Expanding this relationship to linear order near a reference state where $P_o=P_o^{ref}$, $V_{ohc}=V_{ohc}^{ref}$ and $[\kappa_{ohc}]=[\kappa_{ohc}^{ref}]$ yields

$$\dot{Q}=\dot{Q}^{ref}-(g_{hb}P_o^{ref}+g_{ohc})(V_{ohc}-V_{ohc}^{ref})+\alpha([\kappa_{ohc}]-[\kappa_{ohc}^{ref}])+I_{hb}^{max}(P_o-P_o^{ref}). \tag{10}$$

Here g_{hb} and g_{ohc} are conductances associated with the apical and basolateral membranes of the outer hair cell, respectively. The coefficients α and I_{hb}^{max} describe the linear response corresponding to changes in the ion concentration and the open probability of the mechanoelectrical channels, respectively.

We choose the reference state to be a stationary state of the system for a particular set of parameter values such that $\dot{Q}^{ref}=0$. Moreover, we ignore $\alpha([\kappa_{ohc}]-[\kappa_{ohc}^{ref}])$, as it is small within the physiological range of concentration changes.[66] Defining $g\equiv g_{hb}P_o^{ref}+g_{ohc}$ and $V\equiv V_{ohc}-V_{ohc}^{ref}+I_{hb}^{max}P_o^{ref}/g$, the dynamics of the displaced change is written as

$$\dot{Q}=-gV+I_{hb}^{max}P_o. \tag{11}$$

The coefficient I_{hb}^{max} is the current through a hair bundle with open transduction channels when V is zero. This current is driven by an electrochemical gradient across the outer hair cell membrane which depends upon the endocochlear potential.

III. DESCRIPTION OF ACTIVE COCHLEAR MECHANICS

A. Full description of the integrated system

We now combine the components discussed above into an integrated description of the cochlear partition. This description includes the passive mechanics of the partition [Eq. (1) and Eq. (3)], the active motility of the hair bundles [Eq. (5) and Eq. (6)], the electromotile response of the outer hair cells [Eq. (8) and Eq. (9)] and the dynamics of outer hair cell charge [Eq. (11)]. The resulting dynamical equations are

$$m_1\ddot{x}_{hb}-m_2\ddot{x}_{az}+\lambda\dot{x}_{hb}=-K_{gs}(x_{hb}-x_a-DP_o)-(K_{sp}+K_{cp})x_{hb}+K_{12}x_{ohc}+K_{13}x_{az}+K_{14}x_{pz}, \tag{12}$$

$$\lambda_a\dot{x}_a=K_{gs}(x_{hb}-x_a-DP_o)-\gamma f_{max}(1-SP_o), \tag{13}$$

$$\dot{Q}=-\frac{gQ}{C_{ohc}}-gpx_{ohc}+I_{hb}^{max}P_o, \tag{14}$$

and

$$\begin{pmatrix}\lambda_{ohc}\dot{x}_{ohc}\\ m_{az}\ddot{x}_{az}-m_2\ddot{x}_{hb}+\lambda_{az}\dot{x}_{az}\\ m_{pz}\ddot{x}_{pz}+\lambda_{pz}\dot{x}_{pz}\end{pmatrix}=\boldsymbol{K}'\cdot\begin{pmatrix}x_{hb}\\ x_{ohc}\\ x_{az}\\ x_{pz}\end{pmatrix}+\begin{pmatrix}-pQ\\ \mu_{az}P_{ext}\\ \mu_{pz}P_{ext}\end{pmatrix}. \tag{15}$$

The geometric constraints [Eq. (1)] complete the description of the system. Here $\boldsymbol{K}'$ is a 3×4 matrix of elastic coefficients which is obtained by removing the first row of the matrix $\boldsymbol{K}$ defined in Eq. (4). The effective stiffness of the hair bundle is K_{11} [Eq. (4)] and depends upon the stiffness of the hair bundle, the tectorial membrane, the reticular lamina, Deiters' cell and Hensen's cell (Appendix A). We introduce the contribution to this stiffness from the cochlear partition $K_{cp}\equiv\gamma_{11}^2K_{tm}+\gamma_{21}^2K_{rl}+\gamma_{31}^2K_{dc}+\gamma_{41}^2K_{hc}$. such that $K_{11}=K_{gs}+K_{sp}+K_{cp}$. Equations (12)–(15) and Eq. (1) describe the active mechanics of the cochlear partition driven by the pressure difference P_{ext}. A discussion of this complete system is given in Appendix B.

B. Elimination of fast variables

In order to extract the main properties of this system and to keep the analysis simple we consider the overdamped limit and adiabatically eliminate rapidly relaxing variables (x_{ohc}, x_{az} and x_{pz}). In the overdamped limit the relaxation time of the mechanical variables τ_{hb}, τ_a, τ_{ohc}, τ_{az} and τ_{pz} depend upon the damping coefficients. As the values of the damping coefficients λ_{ohc}, λ_{az} and λ_{pz} are not known we may choose them such that τ_{hb}, τ_a and $\tau_Q \gg \tau_{ohc}$, τ_{az} and τ_{pz}, where τ_Q is the relaxation time of the charge displacement. The overdamped limit is first obtained by neglecting the inertial terms in Eqs. (12)–(15). Then we set $\dot{x}_{ohc}=0$, $\dot{x}_{az}=0$ and $\dot{x}_{pz}=0$ and use Eq. (15) to eliminate the fast variables x_{ohc}, x_{az} and x_{pz}. In this limit the time evolution of the three slowest variables is described by

$$\lambda \dot{x}_{hb} = -K_{gs}(x_{hb} - x_a - DP_o) - Kx_{hb} + \mu_{hb}P_{ext} - \gamma_1 pQ, \tag{16}$$

$$\lambda_a \dot{x}_a = K_{gs}(x_{hb} - x_a - DP_o) - \gamma f_{max}(1 - SP_o), \tag{17}$$

$$\dot{Q} = -gp\alpha_1 P_{ext} - \frac{g}{C_{eff}}Q - gp\gamma_1 x_{hb} + I_{hb}^{max}P_o. \tag{18}$$

Equation (16) is similar to the equation for an isolated hair bundle [Eq. (5)] except for one additional term, $-\gamma_1 pQ$, which describes the effect of electromechanical feedback on the hair bundle. The stiffness K, depends on the stiffnesses of all of the structures in the partition and is much larger than the stiffness of an isolated hair bundle due to the fact that it can be dominated by the stiffnesses of the other components of the partition such as the basilar membrane. The effective external force due to the pressure difference across the basilar membrane is $\mu_{hb}P_{ext}$, where μ_{hb} is an effective area. The equation describing the adaptation motors [Eq. (17)] is the same as Eq. (6). Equation (18) describes the change in the charge displacement of the outer hair cells. This may be driven by P_{ext} due to the electromechanical coupling. Moreover, electromotility and the coupling of mechanical elements in the cochlear partition introduce a linear dependence of $\dot{Q}$ on the hair bundle displacement x_{hb}, in addition to the nonlinear dependence associated with the open probability of the transduction channels. Finally, there is a contribution from electromotility to the effective capacitance $C_{eff}=(C_{ohc}^{-1}+\beta_1 p^2)^{-1}$, where the coefficient β_1 is described below.

The dynamics of the other mechanical degrees of freedom $\boldsymbol{x}=(x_{ohc},x_{az},x_{pz},x_{tm},x_{rl},x_{dc},x_{hc})$, are linearly dependent on P_{ext}, Q and x_{hb}. This can be expressed as

$$\boldsymbol{x} = \boldsymbol{\alpha}P_{ext} + \boldsymbol{\beta}pQ + \boldsymbol{\gamma}x_{hb}, \tag{19}$$

where $\boldsymbol{\alpha}$, $\boldsymbol{\beta}$ and $\boldsymbol{\gamma}$ are coefficient vectors. The coefficients K, μ_{hb}, α_i, β_i and γ_i are determined by the geometry and stiffnesses of the cochlear partition.

The elimination of inertial effects is a dramatic simplification. As a result, the dynamics of the system is described by fewer degrees of freedom and a smaller number of coefficients [Eqs. (16)–(18)]. However, these coefficients now have a much more complex dependence on the bare physiological parameters. Note that the inertial effects neglected here become important at the high frequency end of the cochlea (see Appendix B).

C. Electromotile feedback

The effect of electromotility on the dynamics of the hair bundle is described by the feedback term, $-\gamma_1 pQ$, in Eq. (16). This feedback is effectively nonlinear due to the dependence of $\dot{Q}$ on x_{hb} associated with $P_o(x_{hb}-x_a)$ in Eq. (18). In order to understand the nature of this feedback we linearize Eqs. (16)–(18) in the absence of external pressure. To linear order we find

$$\begin{pmatrix} \dot{x}_{hb} \\ \dot{x}_a \\ \dot{Q} \end{pmatrix} = \begin{pmatrix} -\omega_{hb} & K_c/\lambda & -\gamma_1 p/\lambda \\ \omega_a & -\omega_a & 0 \\ I_{hb}^{max}P_o' & -I_{hb}^{max}P_o' & -\omega_Q \end{pmatrix} \begin{pmatrix} x_{hb} \\ x_a \\ Q \end{pmatrix}. \tag{20}$$

Here we define $P_o' \equiv dP_o(x)/dx$, $K_c \equiv K_{gs}(1-DP_o')$ is the gating spring stiffness between the hair bundle and the adaptation motors and $\omega_{hb} \equiv (K-K_{gs}DP_o')/\lambda$, $\omega_a \equiv (K_{gs}(1-DP_o') + \gamma f_{max}SP_o')/\lambda_a$ and $\omega_Q \equiv g/C_{eff}$ are characteristic frequencies associated with x_{hb}, x_a and Q, respectively. We examine the effect of the dynamics of Q on the dynamics of the hair bundle by writing Eq. (20) in the time Fourier domain defined by

$$\tilde{x}(\omega) = \int_{-\infty}^{\infty} e^{-i\omega t}x(t)dt. \tag{21}$$

Elimination of the Fourier amplitude of the charge displacement $\tilde{Q}$, yields an expression for the Fourier amplitude $\tilde{x}_{hb}$, of the hair bundle displacement given by

$$\begin{aligned} i\omega\lambda\tilde{x}_{hb} = &-(i\omega\lambda_{em}(\omega) + K_{em}(\omega) + \omega_{hb}\lambda)\tilde{x}_{hb} \\ &+ (i\omega\lambda_{em}(\omega) + K_{em}(\omega) + K)\tilde{x}_a. \end{aligned} \tag{22}$$

Here $\lambda_{em}(\omega)$ and $K_{em}(\omega)$ are a frequency dependent friction and stiffness, respectively, which result from the electromotile feedback and have the form

$$\lambda_{em}(\omega) = -\frac{\gamma_1 p I_{hb}^{max}P_o'}{\omega^2 + \omega_Q^2}, \tag{23}$$

$$K_{em}(\omega) = -\omega_Q \lambda_{em}(\omega). \tag{24}$$

Note that $\lambda_{em}(\omega)$ has necessarily the opposite sign of $K_{em}(\omega)$ and that their signs are determined by γ_1, which is in turn set by the stiffnesses and geometry of the cochlear partition. For a given geometry, we find that the sign of γ_1 is determined by the ratio K_{tm}/K_{az}, of the tectorial membrane stiffness and the stiffness of the arcuate zone of the basilar membrane [Fig. 2(a)]. Thus we have two possible feedback scenarios to examine, classified by the sign of the feedback. In case A, with $\gamma_1 > 0$, the electromotile feedback contributes negative damping and positive stiffness to the hair bundle while in case B, with $\gamma_1 < 0$, the electromotile effect contributes positive damping and negative stiffness to the hair bundle.

We also find that the feedback is low pass filtered with a corner frequency ω_Q. This low pass filtering of the feedback is the RC time constant problem.[28,40] However, due to cou-

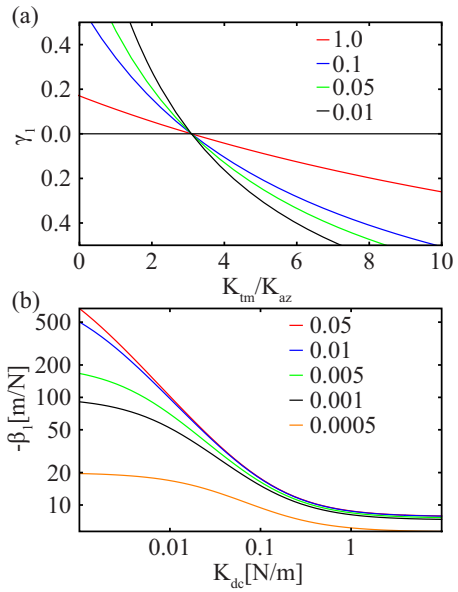

FIG. 2. (Color online) (a) The dimensionless parameter γ_1 describes the coupling of outer hair cell length changes to hair bundle deflections. The sign and magnitude of this parameter determines the nature of the electromotile feedback to the hair bundle. The parameter γ_1 is shown as a function of the ratio K_{tm}/K_{az} of elastic coefficients for different values of K_{az}. Decreasing values of K_{az} result in curves intersecting the γ_1 axis at higher values of γ_1. The K_{az} stiffness values used are: K_{az}=1.0 N/m, 0.1 N/m, 0.05 N/m and 0.01 N/m. (b) The parameter β_1 describes the effect of the electromotile feedback on the effective capacitance C_{eff}. The parameter $-\beta_1$ is shown as a function of the Deiters' cell stiffness K_{dc} for different values of K_{ohc}. These stiffness values are from top to bottom: K_{ohc}=0.05 N/m, 0.01 N/m, 0.005 N/m, 0.001 N/m and 0.0005 N/m.

pling to the surrounding cochlear partition and the electromotile response the corner frequency can in principle be either larger or smaller than g/C_{ohc} depending upon the sign of the coefficient β_1. We find that β_1 is negative and dependents on K_{ohc} and K_{dc} [Fig. 2(b)]. The corner frequency is thus reduced by electromotility.

If the system described by Eqs. (16)–(18) undergoes a Hopf bifurcation, its oscillatory frequency at the bifurcation is $f_c=\omega_c/2\pi$ with

$$\omega_c^2 = \omega_{hb}\omega_a + \omega_{hb}\omega_Q + \omega_a\omega_Q - \frac{K_c\omega_a}{\lambda} + \frac{\gamma_1 p I_{hb}^{max} P_o'}{\lambda}. \quad (25)$$

Equation (25) shows that the resonance frequency of the system is not limited by the slowest internal frequency and in particular can be much larger than the corner frequency ω_Q. The resonance frequency is not set by the properties of the hair bundle alone. The parameters ω_{hb} and γ_1 are strongly dependent upon the stiffness of the basilar membrane and the tectorial membrane [see Fig. 2(a) and the next section]. Moreover, the friction coefficient λ could be dominated by damping due to the deformation of Hensen's cells or the tectorial membrane rather than friction associated with the hair bundle alone. In addition, the electromotile feedback described by p can be used to adjust the critical frequency f_c.

D. Parameter values

We now consider a 10 μm slice of the cochlear partition at the 4 kHz place where most parameter values are well constrained by experimental observations. Many of the parameter values are known from experimental observations, though not in one animal or at all places along the length of the cochlea. We use parameters consistent with observations from the rat, Mongolian gerbil, mouse and guinea pig. Parameter values associated with the dynamical equations Eqs. (16)–(18) are given in Tables I and II. The parameter values for Eq. (19) are given in Tables II and III.

TABLE I. Parameter values for cochlear partition description. Footnotes indicate relevant references.

D	60 nm[a]
δ_{hb}	0.518 nm
A	3.22×10^{29}
g	40 nS[b]
K_{gs}	8×10^{-3} N/m[a]
γ	0.25[a]
p	16 kV/m[c]
C_{ohc}	20 pF[b]

[a]Reference 64.
[b]References 28 and 92.
[c]Reference 25.

We examine the two feedback cases A and B described above. The value of γ_1 is positive in case A and is negative in case B due to different values of the tectorial membrane stiffness K_{tm} [Tables II and III, and Fig. 2(a)]. Moreover, we use different values of three other parameters in case A versus B, namely λ, λ_a and I_{hb}^{max} (Table II). The values of λ and λ_a chosen result in slow hair bundle dynamics in case A and fast hair bundle dynamics in case B. The differences between other parameter values in cases A and B result from the change in K_{tm} [Tables II and III]. A more detailed discussion of the parameter values used is given in Appendix C

IV. SPONTANEOUS OSCILLATIONS AND RESPONSE TO PERIODIC FORCING

A. Case A: Electromotility provides negative damping

1. State diagrams

The state diagrams as a function of S and f_{max} without electromotility (p=0) and with electromotility present (p

TABLE II. Cochlear partition parameter values for case A and case B. Footnotes indicate relevant references. Parameter values for μ_{hb}, K, α_1, β_1 and γ_1 are derived from the geometry and elastic properties of the cochlear partition and are different in cases A and B as the values of K_{tm} are not the same in these cases.

	Case A	Case B
λ	2×10^{-5} Ns/m	5×10^{-7} Ns/m[a]
λ_a	2×10^{-5} Ns/m[b]	5×10^{-7} Ns/m[c]
I_{hb}^{max}	3 nA[d]	25 nA
μ_{hb}	1.05 nm/Pa	1.89 nm/Pa
K	0.103 N/m	0.391 N/m
α_1	−6.91 nm/Pa	−3.88 nm/Pa
β_1	−8.12 m/N	−4.40 m/N
γ_1	0.530	−0.506

[a]Reference 45.
[b]Reference 63.
[c]Reference 64.
[d]Reference 70.

TABLE III. Elastic and geometric coefficients for cases A and B. The different values in A and B result from the difference in K_{tm} only.

	Case A	Case B
α_2	5.57 nm/Pa	2.23 nm/Pa
α_3	6.15 nm/Pa	7.32 nm/Pa
α_4	−3.54 nm/Pa	−1.42 nm/Pa
α_5	−12.8 nm/Pa	−5.12 nm/Pa
α_6	−0.0691 nm/Pa	−0.0388 nm/Pa
α_7	−17.3 nm/Pa	−10.8 nm/Pa
β_2	6.86 m/N	2.74 m/N
β_3	1.61 m/N	3.06 m/N
β_4	−4.36 m/N	−1.74 m/N
β_5	−15.8 m/N	−6.31 m/N
β_6	0.919 m/N	0.956 m/N
β_7	−16.4 m/N	−8.53 m/N
γ_2	1.07	2.21
γ_3	0.206	−0.197
γ_4	1.21	0.485
γ_5	1.35	−1.29
γ_6	0.00530	−0.00506
γ_7	1.13	−1.08

=16 kV/m) are shown in Fig. 3 for case A. Both diagrams have three primary regions where the system is bistable (BI), monostable (MONO) or oscillatory (OSC). The solid lines separating the oscillatory regions from the monostable regions are Hopf bifurcation lines. The transduction channels respond most sensitively to hair bundle motion along the dashed lines where $P_o=1/2$. We consider the behavior of the system at the operating points O_i and $\bar{O}_i$ (circles). The operating points O_i correspond to specific values of S and f_{max} with $p=0$, while the $\bar{O}_i$ are corresponding operating points with electromotility present.

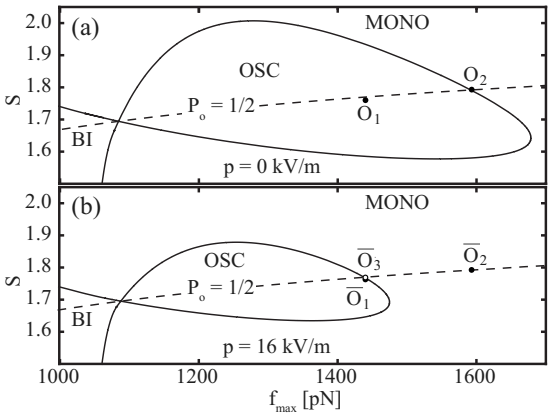

FIG. 3. State diagrams for the dynamical system given in Eqs. (16)–(18) describing the active mechanics of the cochlear partition in case A, where $\gamma_1>0$. The system behavior in the absence of an external stimulus is shown as a function of the maximal force of adaptation motors f_{max} and the strength of the calcium feedback S of hair bundles. Three regions can be distinguished: a region OSC of spontaneous oscillations, a monostable region MONO and a region where the system is bistable BI. The solid line loop indicates a line of Hopf bifurcations. The points $\bar{O}_1$ to $\bar{O}_3$ are different operating points of the system discussed in the text. (a) State diagram in the absence of electromotility ($p=0$). (b) Same state diagram but with electromotility present ($p=16$ kV/m). The operating points correspond to the following parameter values: $S=1.76$ and $f_{max}=1.44$ nN (O_1 and $\bar{O}_1$), $S=1.793$ and $f_{max}=1.593$ nN (O_2 and $\bar{O}_2$), $S=1.77$ and $f_{max}=1.44$ nN ($\bar{O}_3$). The dashed line in (b) and (c) indicates operating points with $P_o=1/2$. [See Tables I and II for parameter values.]

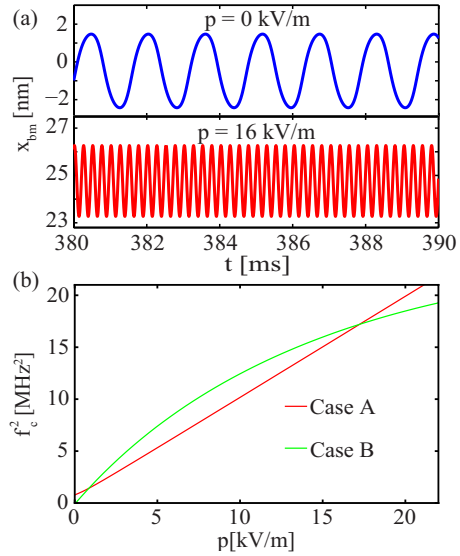

FIG. 4. (Color online) (a) Spontaneous oscillations of the basilar membrane. The displacement of the basilar membrane $x_{bm}=x_{az}+x_{pz}$ is shown as a function of time t when the operating point is in the oscillatory region when there is no electromotility (operating point O_1) and when electromotility is present (operating point $\bar{O}_1$). (b) Spontaneous oscillation frequency. The square of the frequency of spontaneous oscillations at the Hopf bifurcation f_c^2, when $P_o=1/2$, is shown as a function of the electromotility coefficient p for cases A and B.

2. Electromotility increases the spontaneous oscillation frequency and the resonance frequency

The spontaneous displacements of the basilar membrane $x_{bm}(t)=x_{az}(t)+x_{pz}(t)$, as a function of time are shown in Fig. 4(a) at the operating points O_1 and $\bar{O}_1$ which lie in the oscillatory region of the state diagrams shown in Fig. 3. The basilar membrane oscillates spontaneously with a frequency of 0.64 kHz when $p=0$ and with a frequency of 3.98 kHz when electromotility is present with $p=16$ kV/m. The natural frequency of the system as a function of p can be determined analytically at the Hopf bifurcation with $P_o=0.5$ from Eq. (25) [Fig. 4(b)]. This critical frequency behaves as $f_c \sim p^{1/2}$ for large p.

If the system is stimulated with a sinusoidal pressure difference across the basilar membrane $\tilde{P}_{ext}$, at a frequency f, it elicits a vibration of the basilar membrane $\tilde{x}_{bm}$, at the same frequency. The sensitivity $\chi=|\tilde{x}_{bm}/\tilde{P}_{ext}|$ is displayed in Fig. 5(a) for different operating points in the non-oscillatory region at $|\tilde{P}_{ext}|=20$ μPa [We refer to this as 0 dB sound pressure level (SPL) for simplicity]. There is an increase in the frequency where maximum sensitivity occurs when electromotility is present from 0.89 kHz at operating point O_2 to 4.06 kHz at operating point $\bar{O}_2$.

3. Hair bundle motility and electromotility affect the sensitivity

Introducing electromotility at operating point O_2, without changing the other parameters, reduces the sensitivity

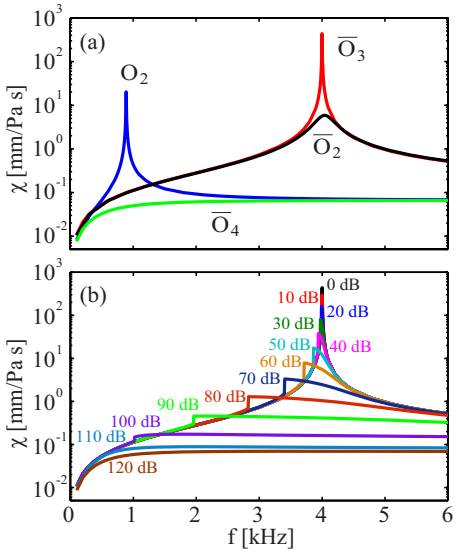

FIG. 5. (Color online) Sensitivity to external sinusoidal pressure stimuli χ in case A as a function of frequency. (a) The sensitivity for a stimulus pressure amplitude of $|\tilde{P}_{ext}|=20$ μPa is shown as a function of frequency f, for different operating points described in Fig. 3. Operating point O_2 is for the case with no electromotility. Operating points $\bar{O}_2$, $\bar{O}_3$ and $\bar{O}_4$ correspond the case with electromotility ($p=16$ kV/m). The adaptation motors are turned off $f_{max}=0$ at operating point $\bar{O}_4$ and in this case the system is bistable. We show the sensitivity at the closed state here. The sensitivity is largest when electromotility is present and when the operating point is near the Hopf bifurcation (operating point $\bar{O}_3$). (b) The sensitivity with electromotility present and adaptation motors on (operating point $\bar{O}_3$) is shown as a function of the stimulus frequency f for different sound pressure levels (0 dB SPL corresponds to 20 μPa.). The frequency at which the peak of the sensitivity occurs and the symmetry of the sensitivity curve decrease as the sound pressure level increases until the curves no longer have a well defined maximum.

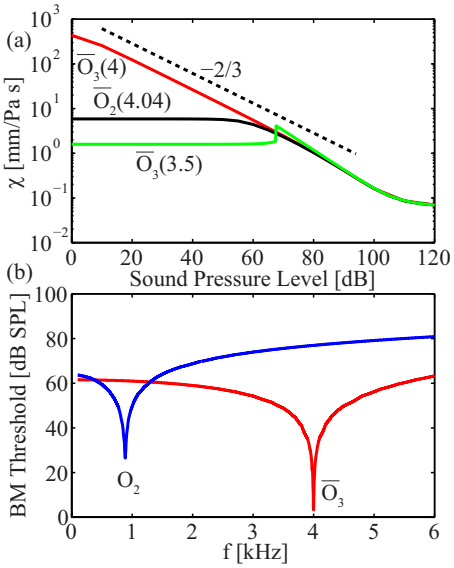

FIG. 6. (Color online) (a) Basilar membrane sensitivity as a function of stimulus sound pressure level. The sensitivities at different operating points and stimulus frequencies are shown as a function of sound pressure level as solid lines. The stimulus frequencies in kHz are shown in parentheses for each operating point. The dashed line indicates the slope of a power law function of the external pressure with a power of −2/3. The largest change in sensitivity over the range of sound input levels shown occurs when the system is stimulated at the resonance frequency corresponding to an operating point close to the Hopf bifurcation [operating point $\bar{O}_3$ (4)]. (b) Basilar membrane tuning curves. The threshold sound pressure levels needed to drive basilar membrane vibrations with $|x_{bm}|>0.4$ nm are shown as a function of frequency f at two different operating points. One curve corresponds to the case without electromotility (operating point O_2) and has a minimum at a frequency of 0.89 kHz. The second curve corresponds to the case with electromotility ($p=16$ kV/m) (operating point $\bar{O}_3$) and has a minimum at a higher frequency of 4 kHz.

[$\bar{O}_2$, Fig. 5(a)]. This reduction is the result of operating point $\bar{O}_2$ being further from the Hopf bifurcation than operating point O_2 (Fig. 3). This can been seen by noting that the relaxation time τ, of the system decreases when moving from O_2 ($\tau=100$ ms) to $\bar{O}_2$ ($\tau=0.8$ ms). However, if we compare O_2 to $\bar{O}_3$, where the relaxation time is the same, we find that electromotility increases the sensitivity.

For a passive hair bundle ($f_{max}=0$) with electromotility present ($\bar{O}_4$), the system is bistable. The maximum sensitivity is now much smaller than at other operating points and there is no peak of sensitivity as a function of frequency [Fig. 5(a)].

4. Nonlinear response

The sensitivity χ, is shown for operating point $\bar{O}_3$ in Fig. 5(b) as a function of stimulus frequency for various sound pressure levels. For $|\tilde{P}_{ext}|$ between 0 dB and 90 dB SPL, χ exhibits a peak at the resonance frequency. As the intensity of the stimulus increases, the magnitude of the peak and the resonance frequency decrease while the width of the peak grows. At intensities larger than 90 dB SPL there is no well defined peak in the sensitivity and the frequency dependence of the sensitivity is similar to the case when adaptation motors are turned off ($f_{max}=0$) [Fig. 5(a)].

The sensitivity as a function of stimulus amplitude exhibits a compressive nonlinearity [Fig. 6(a)]. At 4 kHz the sensitivity at operating point $\bar{O}_3$ obeys $\chi\sim|\tilde{P}_{ext}|^{\nu}$, over several orders of magnitude with $\nu=-2/3$ due to the proximity to a Hopf bifurcation.[14,15] In contrast, the range of the compressive nonlinearity is significantly reduced when the system is stimulated at 3.5 kHz $\bar{O}_3$, or when the operating point is $\bar{O}_2$ (further from the bifurcation) and the system is stimulated at 4.04 kHz.

Calculated tuning curves at O_2 and $\bar{O}_3$ are shown in Fig. 6(b). They display the SPL that elicits a basilar membrane vibration of 0.4 nm in amplitude as a function of frequency. The minimum threshold is 23 dB SPL smaller when electromotility is present ($\bar{O}_3$) than when it is absent (O_2). Furthermore, the quality of the resonance increases from about 20 to 240 and its frequency shifts from 0.89 kHz to 4 kHz as a consequence of the electromotile feedback (Resonance quality is the ratio of the frequency at the minimum threshold to the curve width 10 dB SPL above the minimum).

5. Cochlear partition vibrations

The vibration patterns of the sinusoidally stimulated system are represented using phasor diagrams in Fig. 7. Without electromotility the movement of the mechanical degrees of freedom are in phase with one another Fig. 7(b). Electromo-

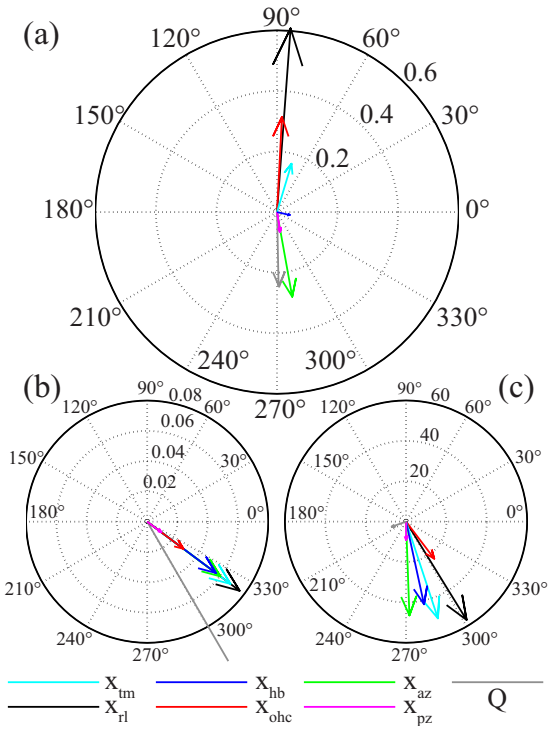

FIG. 7. (Color online) Vibration pattern of the cochlear partition in case A. The vibration pattern of the components of the cochlear partition is shown using phasor diagrams. Each arrow represents the motion of a component of the cochlear partition defined in Fig. 1(a) relative to a sinusoidal sound pressure stimulus. The length of each arrow indicates the amplitude of the corresponding displacement and the angle relative to 0° indicates the phase of the displacement with respect to the stimulation. The circular dashed lines indicate the magnitude of mechanical displacements in nm or the magnitude of charge displacement in units of 10^{-14} C. (a) Vibration pattern with electromotility present (operating point $\bar{O}_3$) for a 0 dB SPL amplitude and 4 kHz frequency stimulus. The elongation of the outer hair cell leads the displacement of the hair bundle by about 90°. (b) Vibration pattern without electromotility present (operating point $\bar{O}_2$) for a 0 dB SPL amplitude and 0.89 kHz frequency stimulus. All of the mechanical displacements are in phase with one another. (c) Vibration pattern with electromotility present (operating point $\bar{O}_3$) for a 120 dB SPL amplitude and 4 kHz frequency stimulus. All of the mechanical displacements are approximately in phase with one another.

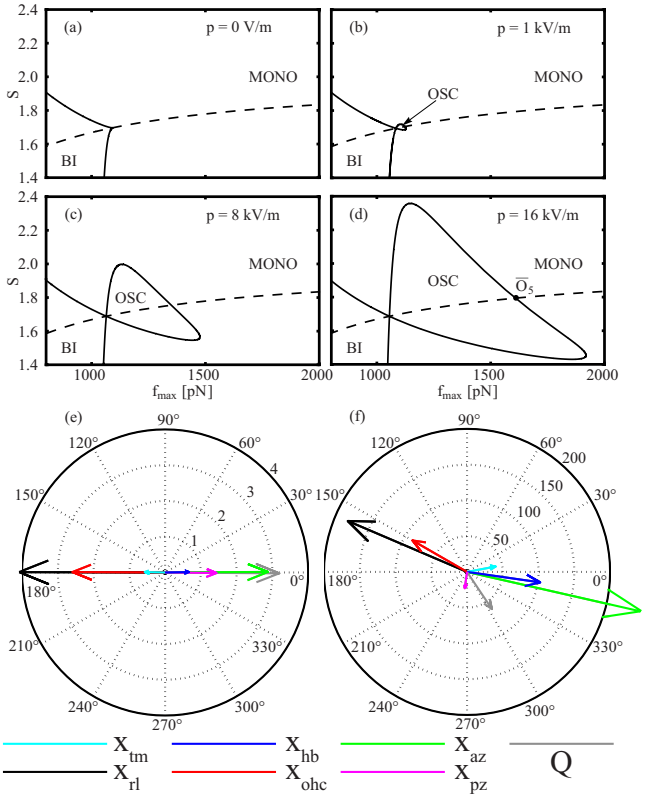

FIG. 8. (Color online) [(a)–(d)] State diagrams for the dynamical system given in Eqs. (16)–(18) describing the active mechanics of the cochlear partition in case B, where $\gamma_1 < 0$. The system's behavior in the absence of an external stimulus is shown as a function of f_{max} and S for different values of the electromotility coefficient p. (a) There is no Hopf bifurcation when $p = 0$. [(c) and (d)] A loop of Hopf bifurcations appears for $p > 0$ and grows in size as p increases. The operating point $\bar{O}_5$ is at $S = 1.80$ and $f_{max} = 1.61$ nN corresponding to a system relaxation time of $\tau = 100$ ms. [(e) and (f)] Vibration pattern of the cochlear partition in case B. Vibration pattern with electromotility present ($p = 16$ kV/m) (operating point $\bar{O}_5$) at a stimulus frequency of 4 kHz. (e) The amplitude of the stimulus is 0 dB SPL. The contraction of the outer hair cell is in phase with the displacement of the hair bundle. (f) The amplitude of the stimulus is 120 dB SPL.

tility introduces relative phase differences between these variables [Fig. 7(a)]. Negative hair bundle damping results from outer hair cell elongation being in phase with the velocity of the hair bundle (velocity leads displacement by 90°). The mechanical displacement variables move into phase with respect to one another for large stimuli [Fig. 7(c)], similar to the case without electromotility.

B. Case B: Electromotility provides negative stiffness

1. State diagrams

State diagrams of case B for various values of p are shown in Fig. 8. For $p = 0$ there is no oscillatory region due to the large tectorial membrane stiffness used [Fig. 8(a)]. As p is increased from zero, an oscillatory region appears and grows in size due to the negative stiffness provided by the electromotile feedback.

2. Both electromotility and hair bundle motility tune the oscillation frequency

The critical frequency f_c at the bifurcation, for $P_o = 1/2$, is shown as a function of p in Fig. 4(b). The frequency grows initially due to the increase in the values of f_{max} and S required to maintain the operating point on the Hopf bifurcation line at $P_o = 1/2$. However, f_c attains a maximum at $p = 42$ kV/m and vanishes at $p = 100$ kV/m as electromotility decreases f_c when $\gamma_1 < 0$ [see Eq. (25)]. At the operating point $\bar{O}_5$ in Fig. 8(d) the resonance frequency is 4.05 kHz. At this operating point near the bifurcation the system exhibits the same generic features of high sensitivity, compressive nonlinearity and sharp frequency tuning described in case A.

3. Cochlear partition vibrations

The vibration patterns of the system in response to external pressure stimuli at operating point $\bar{O}_5$ are shown in Fig. 8. At low stimulus levels electromotile feedback provides negative stiffness to the hair bundle. However, at high stimulus levels negative stiffness is reduced as the pressure force $\mu_{hb} P_{ext}$, dominates the electromotile feedback force

$-\gamma_1 pQ$ [see Eq. (16)]. Figure 8 shows the stimulus amplitude dependence of the vibration pattern due to nonlinearities in the system. The connection between negative stiffness and the vibration pattern can best be seen at low levels of input where the contraction of the outer hair cell results in a force on the hair bundle in phase with its deflection [Fig. 8(e)].

V. CONCLUSIONS

In this work we address the interplay between active hair bundle movements and electromotile feedback in a slice of the cochlear partition, which is described by three coupled differential equations [Eqs. (16)–(18)]. We distinguish two possible cases: in case A electromotility provides negative damping to the hair bundle and in case B it results in negative stiffness. In case A spontaneous oscillations are possible in the absence of electromotility. In this case the main role of electromotility is to allow the combined system to achieve a higher frequency of spontaneous oscillation and resonance as compared to the hair bundle alone. Furthermore, electromotility also increases the sensitivity to periodic stimuli and it sharpens the frequency tuning. In case B both hair bundle motility and electromotility are required for spontaneous oscillations to exist. In this case, electromotile feedback decreases the frequency of oscillations due to positive damping. If the system operates in the vicinity of a Hopf bifurcation both cases A and B exhibit similar properties of nonlinear amplification and frequency selectivity. Which case is of relevance for the cochlea? There is experimental evidence in support of case A. A decrease in the characteristic frequency and a broadening of the frequency tuning have been reported when electromotility is absent in a mutant mouse.[67] Moreover, some of the parameters chosen to generate case B appear to be unphysiological (see Appendix C). We therefore suggest that the cochlea operates, at least at the 4 kHz place, under conditions similar to case A, where electromotile feedback provides negative damping.

Although the electromotile feedback is limited by the RC time constant we find that this is not a problem at the characteristic place described here. The 4 kHz resonance frequency of the partition is much larger than the corner frequency $\omega_Q/(2\pi)=0.3$ kHz in both case A and case B corresponding to the membrane time constant. As a result the electromotile feedback is attenuated, but it can still effectively drive basilar membrane vibrations at 4 kHz and boost mechanical amplification. Cochlear partition inertia could play a role at higher frequency locations along the cochlea in mitigating the attenuation of electromotile feedback (see Appendix B).

The contractile electromotile force of the outer hair cell soma has two opposing effects on the hair bundle. First, it pulls Corti's arch (formed by the two pillar cells), toward the tectorial membrane by acting directly on the basilar membrane. This results in a force on the hair bundle in the positive direction, as the pivot point of the reticular lamina moves closer to the tectorial membrane (Fig. 1). Second, this electromotile force pulls the reticular lamina downwards. This induces a negative force on the hair bundle. The direction of the net force on the hair bundle depends on the relative importance of these two effects, which in turn depend upon the stiffnesses of the components to which the hair bundle is coupled. In case B, where electromotility provides negative stiffness and the tectorial membrane is stiff (Table V), the electromotile force acts in the direction of positive hair bundle displacements, thus producing negative stiffness [Fig. 8(e)]. In case A the net force on the hair bundle due to outer hair cell elongation is in phase with the velocity of the hair bundle yielding negative hair bundle damping [Fig. 7(a)]. Both of these scenarios differ from the previously hypothesized effect of electromotility on the cochlear partition.[68] However, the relative motions of the reticular lamina, tectorial membrane and basilar membrane with respect to the change in length of the outer hair cell [Fig. 7(a) and Fig. 8(e)] obtained here are consistent with experimental observations of cochlear partition vibrations.[60–62]

Our work shows that the inertia of the partition is not necessary for frequency tuning. This implies that a traveling wave with a nonlinear response at a characteristic place can result from inertialess Hopf oscillators,[69] and that the resonance frequency is set by the combination of hair bundle dynamics and electromotility. Indeed, our description indicates how tonotopic variation in the properties of the partition, such as the maximum hair bundle current I_{hb}^{max} or the electromotility coefficient p, could regulate the place frequency map within the cochlea [Eq. (25) and see Appendix C].

In our description, the cochlear amplifier gets its energy input from the work of hair bundle adaptation motors as well as the electrochemical gradients across the outer hair cell membrane. In the presence of electromotility, it is possible to turn the hair bundle motors off ($f_{max}=0$) and to choose system parameters such that spontaneous oscillations occur for passive hair bundles (see Appendix D). However, for this to be possible I_{hb}^{max} needs to be one to two orders of magnitude larger than the physiological estimate[70] (see Appendix C).

The responses of the cochlear partition slice to external sound stimuli discussed here are related to local experimental observations of the cochlear traveling wave (Figs. 5 and 6).[4–6,67] However, we overestimate the maximum sensitivity and the sharpness of the resonance at operating point $\bar{O}_3$ as we have not corrected for the gain of the middle ear[71] and we do not take the effects of fluctuations into account.[63] In addition, the compressive nonlinearity we describe at this operating point is modified by the traveling wave[69] and by fluctuations.[44] Finally, the traveling wave can modulate cochlear responses to be more asymmetric at low sound pressure levels than the responses we calculate.[4,5,49]

In vivo a homeostatic mechanism may regulate the system to operate in the proximity of a Hopf bifurcation.[14] For example, such a mechanism could be based on adjustment of hair bundle motility by changing f_{max} or on regulation of electromotility by varying p. Since outer hair cells receive efferent nerve fibers from the brain such mechanisms could be controlled by the central nervous system.[1,2,72,73] Overall our description indicates that electromotility and hair bundle motility work together to provide the mammalian ear with its remarkable signal detection properties.

APPENDIX A: GEOMETRIC CONSTRAINTS AND PASSIVE LINEAR MICROMECHANICS

1. Passive linear mechanics

Equation (3) can be derived systematically by writing the Lagrange function for the system described by the geometry of masses and springs shown in Fig. 1. This Lagrangian is given by

$$\begin{aligned} L = {} & \tfrac{1}{2}M_{\mathrm{az}}\dot{x}_{\mathrm{az}}^2 + \tfrac{1}{2}M_{\mathrm{pz}}\dot{x}_{\mathrm{pz}}^2 + \tfrac{1}{2}M_{\mathrm{tm}}(\gamma_{11}\dot{x}_{\mathrm{hb}} + \gamma_{13}\dot{x}_{\mathrm{az}})^2 \\ & - \tfrac{1}{2}(K_{\mathrm{sp}} + K_{\mathrm{gs}})x_{\mathrm{hb}}^2 - \tfrac{1}{2}K_{\mathrm{ohc}}x_{\mathrm{ohc}}^2 - \tfrac{1}{2}K_{\mathrm{az}}x_{\mathrm{az}}^2 - \tfrac{1}{2}K_{\mathrm{pz}}x_{\mathrm{pz}}^2 \\ & - \tfrac{1}{2}K_{\mathrm{hc}}(\gamma_{41}x_{\mathrm{hb}} + \gamma_{43}x_{\mathrm{az}} + \gamma_{44}x_{\mathrm{pz}})^2 - \tfrac{1}{2}K_{\mathrm{tm}}(\gamma_{11}x_{\mathrm{hb}} + \gamma_{13}x_{\mathrm{az}})^2 \\ & - \tfrac{1}{2}K_{\mathrm{rl}}(\gamma_{21}x_{\mathrm{hb}} + \gamma_{23}x_{\mathrm{az}})^2 \\ & - \tfrac{1}{2}K_{\mathrm{dc}}(\gamma_{31}x_{\mathrm{hb}} - x_{\mathrm{ohc}} + \gamma_{33}x_{\mathrm{az}} + \gamma_{34}x_{\mathrm{pz}})^2. \end{aligned} \tag{A1}$$

Here M_{az}, M_{pz} and M_{tm} are the masses of the arcuate zone, pectinate zone and tectorial membrane respectively and the K_{ij} are stiffness. In writing the Lagrangian, we have already made use of geometrical constraints on the system [Eqs. (1) and (2)].

Rayleigh's dissipation function describes the friction forces on the system and we write it as

$$F = \tfrac{1}{2}\lambda\dot{x}_{\mathrm{hb}}^2 + \tfrac{1}{2}\lambda_{\mathrm{ohc}}\dot{x}_{\mathrm{ohc}}^2 + \tfrac{1}{2}\lambda_{\mathrm{az}}\dot{x}_{\mathrm{az}}^2 + \tfrac{1}{2}\lambda_{\mathrm{pz}}\dot{x}_{\mathrm{pz}}^2, \tag{A2}$$

where the λ are friction coefficients. The dynamic equations involving force balances of elastic, inertial, friction and external forces can be obtained from Lagrange's equation as[74]

$$\frac{d}{dt}\left(\frac{dL}{d\dot{x}}\right) - \frac{dL}{dx} + \frac{dF}{d\dot{x}} = F_{\mathrm{ext}}, \tag{A3}$$

Here, x is any of the independent dynamic variables $(x_{\mathrm{hb}}, x_{\mathrm{ohc}}, x_{\mathrm{az}}, x_{\mathrm{pz}})$ and F_{ext} is the corresponding element from the force vector $(0, 0, \mu_{\mathrm{az}}P_{\mathrm{ext}}, \mu_{\mathrm{pz}}P_{\mathrm{ext}})$. This leads to Eq. (3) where the masses are given by $m_1 = \gamma_{11}^2 M_{\mathrm{tm}}$, $m_2 = -\gamma_{11}\gamma_{13}M_{\mathrm{tm}}$, $m_{\mathrm{az}} = M_{\mathrm{az}} + \gamma_{13}^2 M_{\mathrm{tm}}$ and $m_{\mathrm{pz}} = M_{\mathrm{pz}}$. The stiffnesses in Eq. (4) also result from Eq. (A3) and are linear combinations of the stiffness parameters in the Lagrangian. For example, $K_{11} = K_{\mathrm{gs}} + K_{\mathrm{sp}} + \gamma_{11}^2 K_{\mathrm{tm}} + \gamma_{21}^2 K_{\mathrm{rl}} + \gamma_{31}^2 K_{\mathrm{dc}} + \gamma_{41}^2 K_{\mathrm{hc}}$.

2. Geometric constraints

In this section we show how the geometric constraints are obtained which are used in the Lagrangian for the passive system [Eq. (A1)]. The variables which describe the deformation of the cochlear partition are the angles θ_{tm}, θ_{rl}, θ_{hb}, θ_{az} and θ_{pz} and the spring lengths x_{ohc}, x_{dc} and x_{hc}. The angular variables are related to the displacements x_{tm}, x_{rl}, x_{hb}, x_{az} and x_{pz}: $x_{\mathrm{tm}} = z_{\mathrm{tm}}\sin(\theta_{\mathrm{tm}})$, $x_{\mathrm{rl}} = z_{\mathrm{rl}}\sin(\theta_{\mathrm{rl}})$, $x_{\mathrm{hb}} = l_{\mathrm{hb}}\sin(\theta_{\mathrm{hb}})$, $x_{\mathrm{az}} = (z_{\mathrm{az}} + z_{\mathrm{pz}})\sin(\theta_{\mathrm{az}})$ and $x_{\mathrm{pz}} = z_{\mathrm{pz}}\sin(\theta_{\mathrm{pz}})$, where the beam lengths z_{tm}, z_{rl}, l_{hb}, z_{az} and z_{pz} are constant, see Fig. 1. The geometry of the partition introduces the following geometric relations:

$$\begin{aligned} l_{\mathrm{hb}}^2 = {} & \left(z_{\mathrm{tm}}\cos(\theta_{\mathrm{tm}}) - z_{\mathrm{hb}}\cos(\theta_1) - z_{\mathrm{ipc}} - \frac{y_{\mathrm{pc}}\sin(\theta_2)}{\sin(\theta_{\mathrm{ipc}})}\right)^2 \\ & + \left(z_{\mathrm{tm}}\sin(\theta_{\mathrm{tm}}) - z_{\mathrm{hb}}\sin(\theta_1) + y_{\mathrm{ooC}} - \frac{y_{\mathrm{pc}}\cos(\theta_2)}{\sin(\theta_{\mathrm{ipc}})}\right)^2, \end{aligned} \tag{A4}$$

$$\begin{aligned} z_{\mathrm{tm}}^2 = {} & \left(l_{\mathrm{hb}}\sin(\theta_3) + z_{\mathrm{hb}}\cos(\theta_1) + z_{\mathrm{ipc}} + \frac{y_{\mathrm{pc}}\sin(\theta_2)}{\sin(\theta_{\mathrm{ipc}})}\right)^2 \\ & + \left(l_{\mathrm{hb}}\cos(\theta_3) + z_{\mathrm{hb}}\sin(\theta_1) - y_{\mathrm{ooC}} + \frac{y_{\mathrm{pc}}\cos(\theta_2)}{\sin(\theta_{\mathrm{ipc}})}\right)^2, \end{aligned} \tag{A5}$$

$$\begin{aligned} (x_{\mathrm{ohc}} + x_{\mathrm{dc}})^2 = {} & (y_{\mathrm{pc}} + z_{\mathrm{hb}}\sin(\theta_{\mathrm{rl}}) - z_1\tan(\theta_{\mathrm{pz}}))^2 \\ & + \left(z_{\mathrm{ohc}} - z_1\frac{1}{\cos(\theta_{\mathrm{pz}})}\right)^2 - 2(y_{\mathrm{pc}} + z_{\mathrm{hb}}\sin(\theta_{\mathrm{rl}}) \\ & - z_1\tan(\theta_{\mathrm{pz}})) \times \left(z_{\mathrm{ohc}} - z_1\frac{1}{\cos(\theta_{\mathrm{pz}})}\right) \\ & \times\cos(\pi/2 - \theta_{\mathrm{pz}}), \end{aligned} \tag{A6}$$

$$\begin{aligned} x_{\mathrm{hc}}^2 = {} & (y_{\mathrm{pc}} + z_{\mathrm{rl}}\sin(\theta_{\mathrm{rl}}) - z_2\tan(\theta_{\mathrm{pz}}))^2 + \left(z_{\mathrm{pz}} - z_2\frac{1}{\cos(\theta_{\mathrm{pz}})}\right)^2 \\ & - 2(y_{\mathrm{pc}} + z_{\mathrm{rl}}\sin(\theta_{\mathrm{rl}}) - z_2\tan(\theta_{\mathrm{pz}})) \\ & \times\left(z_{\mathrm{pz}} - z_2\frac{1}{\cos(\theta_{\mathrm{pz}})}\right)\cos(\pi/2 - \theta_{\mathrm{pz}}), \end{aligned} \tag{A7}$$

where

$$y_{\mathrm{pc}} = z_{\mathrm{az}}\left(\frac{1}{\tan(\theta_{\mathrm{ipc}})} + \frac{1}{\tan(\theta_{\mathrm{opc}})}\right)^{-1}, \tag{A8}$$

$$\theta_1 = \theta_{\mathrm{rl}} + \theta_{\mathrm{az}}, \tag{A9}$$

$$\theta_2 = \pi/2 - \theta_{\mathrm{ipc}} - \theta_{\mathrm{az}}, \tag{A10}$$

$$\theta_3 = \theta_{\mathrm{hb}} - \theta_{\mathrm{rl}} - \theta_{\mathrm{az}}, \tag{A11}$$

$$z_1 = z_{\mathrm{hb}}\cos(\theta_{\mathrm{rl}}) - \frac{y_{\mathrm{pc}}}{\tan(\theta_{\mathrm{opc}})}, \tag{A12}$$

$$z_2 = z_{\mathrm{rl}}\cos(\theta_{\mathrm{rl}}) - \frac{y_{\mathrm{pc}}}{\tan(\theta_{\mathrm{opc}})}. \tag{A13}$$

These nonlinear geometric constraints can be linearized around a reference state. Using the fact that the beam lengths are constant, we find to linear order

$$0 = \frac{\partial l_{\mathrm{hb}}}{\partial\theta_{\mathrm{tm}}}\delta\theta_{\mathrm{tm}} + \frac{\partial l_{\mathrm{hb}}}{\partial\theta_{\mathrm{rl}}}\delta\theta_{\mathrm{rl}} + \frac{\partial l_{\mathrm{hb}}}{\partial\theta_{\mathrm{az}}}\delta\theta_{\mathrm{az}}, \tag{A14}$$

$$0 = \frac{\partial z_{\mathrm{tm}}}{\partial\theta_{\mathrm{hb}}}\delta\theta_{\mathrm{hb}} + \frac{\partial z_{\mathrm{tm}}}{\partial\theta_{\mathrm{rl}}}\delta\theta_{\mathrm{rl}} + \frac{\partial z_{\mathrm{tm}}}{\partial\theta_{\mathrm{az}}}\delta\theta_{\mathrm{az}}, \tag{A15}$$

$$\delta x_{dc} + \delta x_{ohc} = \frac{\partial (x_{dc} + x_{ohc})}{\partial \theta_{rl}} \delta\theta_{rl} + \frac{\partial (x_{dc} + x_{ohc})}{\partial \theta_{pz}} \delta\theta_{pz}, \tag{A16}$$

$$\delta x_{hc} = \frac{\partial x_{hc}}{\partial \theta_{rl}} \delta\theta_{rl} + \frac{\partial x_{hc}}{\partial \theta_{pz}} \delta\theta_{pz}, \tag{A17}$$

where $\delta\theta_{tm} = \theta_{tm} - \theta_{tm}^{ref}$, $\delta\theta_{rl} = \theta_{rl} - \theta_{rl}^{ref}$, $\delta\theta_{hb} = \theta_{hb} - \theta_{hb}^{ref}$, $\delta\theta_{az} = \theta_{az} - \theta_{az}^{ref}$, $\delta\theta_{pz} = \theta_{pz} - \theta_{pz}^{ref}$, $\delta x_{ohc} = x_{ohc} - x_{ohc}^{ref}$, $\delta x_{dc} = x_{dc} - x_{dc}^{ref}$ and $\delta x_{hc} = x_{hc} - x_{hc}^{ref}$. The reference state values for the angles are defined in Fig. 1(b). For small angular changes, the changes in the beam displacements are: $\delta x_{tm} = z_{tm}\delta\theta_{tm}$, $\delta x_{rl} = z_{rl}\delta\theta_{rl}$, $\delta x_{hb} = l_{hb}\delta\theta_{hb}$, $\delta x_{az} = (z_{az} + z_{pz})\delta\theta_{az}$ and $\delta x_{pz} = z_{pz}\delta\theta_{pz}$.

Using the relations Eqs. (A14)–(A17) we express the displacements δx_{tm}, δx_{rl}, δx_{dc} and δx_{hc} in terms of the other displacements, see Eq. (1). In the main text, we drop the "δ" to simplify the notion. The parameters γ_{ij} in Eq. (2) are functions of the geometric parameters in Eqs. (A4)–(A13) and can be found using Eqs. (A14)–(A17)

APPENDIX B: FULL SYSTEM DYNAMICS

The full system dynamics, given by Eqs. (12)–(15), may be written in the Fourier domain as

$$H_{hb}\tilde{x}_{hb} = K_{gs}(D\tilde{P}_o + \tilde{x}_a) - \frac{H_4^{(A)}K_1K_2}{H_5^{(A)}}\tilde{x}_{hb} - m_2\omega^2\tilde{x}_{az} - \frac{H_4^{(B)}K_3}{H_5^{(A)}}p\tilde{Q} + \frac{H_4^{(C)}K_4}{H_5^{(A)}}\mu_1\tilde{P}_{ext}, \tag{B1}$$

$$H_a\tilde{x}_a = -K_{gs}(D\tilde{P}_o - \tilde{x}_{hb}) - \gamma f_{max}(2\pi\delta(\omega) - S\tilde{P}_o), \tag{B2}$$

$$H_Q\tilde{Q} = -\frac{H_4^{(B)}K_3}{H_5^{(A)}}gp\tilde{x}_{hb} - \frac{H_4^{(D)}}{H_5^{(A)}}gp^2\tilde{Q} - \frac{H_2^{(A)}K_5}{H_5^{(A)}}gp\mu_2\tilde{P}_{ext} + I_{hb}^{max}\tilde{P}_o, \tag{B3}$$

and

$$\tilde{x}_{ohc} = \frac{H_4^{(B)}K_3}{H_5^{(A)}}\tilde{x}_{hb} + \frac{H_4^{(D)}}{H_5^{(A)}}p\tilde{Q} + \frac{H_2^{(A)}K_5}{H_5^{(A)}}\mu_2\tilde{P}_{ext}, \tag{B4}$$

$$\tilde{x}_{az} = \frac{H_5^{(B)}}{H_5^{(A)}}\tilde{x}_{hb} + \frac{H_2^{(B)}}{H_5^{(A)}}p\tilde{Q} + \frac{H_3^{(A)}K_6}{H_5^{(A)}}\mu_3\tilde{P}_{ext}, \tag{B5}$$

$$\tilde{x}_{pz} = \frac{H_3^{(B)}K_7}{H_5^{(A)}}\tilde{x}_{hb} + \frac{H_2^{(C)}}{H_5^{(A)}}p\tilde{Q} + \frac{H_3^{(C)}K_8}{H_5^{(A)}}\mu_4\tilde{P}_{ext}. \tag{B6}$$

Here $H_{hb} = -m_1\omega^2 + \lambda i\omega + K_{gs} + K_{sp} + K_{cp}$, $H_a = \lambda_a i\omega + K_{gs}$, $H_Q = i\omega + g/C_{ohc}$, $H_n = \Sigma_{j=0}^{n} A_j (i\omega)^j$, K_n are stiffnesses and μ_n are effective areas. The constants A_j are functions of the stiffnesses, masses and damping coefficients in Eqs. (12)–(15).

Adiabatic elimination corresponds to the case where the H_n are evaluated for $\omega = 0$ in Eqs. (B1)–(B6). After taking the overdamped limit and adiabatic elimination the H_n are constants independent of masses and damping coefficients.

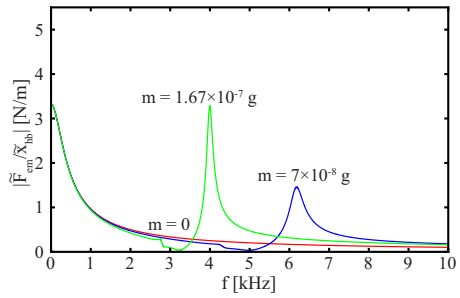

FIG. 9. (Color online) Frequency dependence of the electromotile feedback. The frequency dependence of electromotile feedback is shown by plotting $|\tilde{F}_{em}/\tilde{x}_{hb}|$ as a function of frequency f, where $\tilde{F}_{em}$ is the electromotile feedback force. Each curve corresponds to different values of the tectorial membrane and basilar membrane masses. The masses of the basilar membrane zones and the tectorial membrane are the same (denoted by m) such that the inertial terms are given by $m_{az} = (1 + \gamma_{13}^2)m$, $m_{pz} = m$ and $m_2 = -\gamma_{11}\gamma_{13}m$, where the values of m are given in the figure. When m is not zero there is a resonance in the electromotile feedback. This position of this resonance is associated primarily with the arcuate zone of the basilar membrane. For all curves we use the parameters from case A given in Tables I and II. In addition we use $\lambda_{ohc} = \lambda_{az} = \lambda_{pz} = 10^{-7}$ Ns/m and $P_o = 1/2$.

The most general form of the electromotile feedback can be found by substituting Eq. (B3) into (B1). The force exerted on the hair bundle by electromotility when $\tilde{P}_{ext} = 0$ is given to linear order by

$$\tilde{F}_{em} = \frac{(gK_3pH_4^{(B)}/H_5^{(A)} - I_{hb}^{max}P_o')K_3pH_4^{(B)}}{(i\omega + g/C_{ohc})H_5^{(A)} + gp^2H_4^{(D)}}\tilde{x}_{hb}. \tag{B7}$$

The force $\tilde{F}_{em}$ depends upon the masses m_{az}, m_{pz} and m_2 as well as the damping coefficients λ_{ohc}, λ_{az} and λ_{pz}. We plot $|\tilde{F}_{em}/\tilde{x}_{hb}|$ as a function of frequency $f = \omega/(2\pi)$, in Fig. 9 for three different values of the mass m where $m_{az} = (1 + \gamma_{13}^2)m$, $m_{pz} = m$, and $m_2 = -\gamma_{11}\gamma_{13}m$ for simplicity (see Appendix A). When $m = 0$ the electromotile force is severely attenuated at 4 kHz due to the low pass filtering associated with the RC time constant.

Experimental observations indicate that the bare values of the basilar membrane mass and the tectorial membrane mass are at most 7×10^{-8} g for a 10 μm slice of the cochlear partition.[56] Using $m = 7 \times 10^{-8}$ g we find a resonance at 6.2 kHz. However, the effect of basilar membrane inertia on the electromotile feedback is negligibly small near 4 kHz. If we choose $m_{bm} = 1.67 \times 10^{-7}$ g there is an inertial resonance at 4 kHz which compensates for the RC low pass filtering. The frequency of this inertial resonance is most sensitive to the value of the arcuate zone mass. Thus it may be possible to overcome the RC time constant problem at high frequencies if a basilar membrane resonance is close to that of the active cochlear partition.

At low frequencies the electromotile feedback force has the form

$$\tilde{F}_{em} \approx \frac{\gamma_1 p(gp\gamma_1 - I_{hb}^{max}P_o')}{i\omega + g/C_{ohc} + gp^2\beta_1}. \tag{B8}$$

Equation (B8) may be simplified by using the approximation $I_{hb}^{max}P_o' - gp\gamma_1 \approx I_{hb}^{max}P_o'$ yielding the electromotile feedback terms in Eq. (22). Electromotile feedback is low pass filtered by the RC membrane time constant in this case, but the mag-

TABLE IV. Cochlear partition dimensions. Lengths in μm. Parameters are defined in Fig. 1.

z_{hb}	40[a]
z_{tm}	165[a]
z_{ohc}	25.6[a,b]
l_{hb}	2.8[a]
y_{ooC}	97.2[a]
θ_{ipc}	76°[b]
θ_{rl}^{ref}	20°[b]
θ_{az}^{ref}	7.2°[a,b]
θ_{tm}^{ref}	−0.3°[a,b]
z_{pz}	92.5[b]
z_{ipc}	122[b]
z_{rl}	90[a,b]
z_{az}	83.7[b]
x_{dc}^{ref}	64.2[a,b]
θ_{opc}	47°[b]
θ_{hb}^{ref}	0°[a]
θ_{pz}^{ref}	0°[d]

[a]Reference 58.
[b]Reference 57.
[c]Reference 56.
[d]Assumed.

nitude of the feedback is sufficiently large at 4 kHz to have a big effect on the behavior of the cochlear partition.

APPENDIX C: DISCUSSION OF PARAMETER VALUES

1. Geometry

The geometry of this system is determined by a set of experimental measurements on unfixed cochleae from the Mongolian gerbil (*Meriones unguiculatus*)[56–58] (Table IV, Fig. 1). We note that while there are unknown variations in these geometric parameters the requirement of geometric consistency serves to constrain their possible values.

2. Stiffnesses

The stiffnesses of the components of the system may be estimated from experimental observations of their deflections due to point probes.[75–80] We interpret these measurements within the context of our approximation for the movement of the basilar membrane (up to its mid-point between the spiral lamina and the spiral ligament) as two rigid beams which pivot about the connection of the basilar membrane to the spiral lamina and the base of the outer pillar cell (Fig. 1). Measurements of basilar membrane stiffness in the 4 kHz region yield values in range from 5×10^{-2} N/m to 5×10^{-1} N/m.[75–80] We use the most recent values for basilar membrane stiffnesses for the cochlea of the gerbil.[80] Several studies of the tectorial membrane point stiffness have been made.[81–84] However, the interpretation of these measurements is difficult as the tectorial membrane appears to be quite inhomogeneous.[82] Assuming that the tectorial membrane is homogeneous we estimate the tectorial membrane stiffness range at the 4 kHz place to be 10^{-2} N/m to 5×10^{-1} N/m.[81–83] We examine the behavior of the system when the tectorial membrane stiffness is 10^{-2} N/m (case A) and when it is 5×10^{-1} N/m (case B). No measurements of the stiffness of Deiters' cell are available. We choose its stiffness in order to maximize the outer hair cell corner frequency ω_Q, [Fig. 2(b)]. Order of magnitude estimates are available for the stiffnesses of most of the other components of the system (Table V).

TABLE V. Stiffnesses in N/m.

K_{tm}	0.01(A)/0.5(B)
K_{az}	0.05[a]
K_{sp}	0.005[b]
K_{rl}	0.005[c]
K_{dc}	1
K_{pz}	0.05[a]
K_{hc}	0.01[d]
K_{ohc}	0.01[e]

[a]Reference 80.
[b]Reference 64.
[c]Reference 94.
[d]Reference 93.
[e]References 86 and 38.

3. Damping

The values for the damping coefficients are uncertain. In case A we choose $\lambda=2\times10^{-5}$ Ns/m in order to take into account additional damping of the cochlear partition. This value is large compared to the values corresponding to free-standing hair bundles.[63,64] The value of $\lambda_a=2\times10^{-5}$ Ns/m previously associated with adaptation motors is also used.[63] In case B the damping coefficients $\lambda=5\times10^{-7}$ Ns/m and $\lambda_a=5\times10^{-7}$ Ns/m are chosen to be much smaller as compared to case A in order to tune the system to 4 kHz, leading to faster hair bundle dynamics, similar to the values used for individual rat hair cells.[64] The value for λ used in this case is also close in magnitude to an estimate of viscous damping in the subtectorial space.[45]

4. Hair bundle

The parameter values we use for the hair bundles are based on an application of the model described in Eqs. (5)–(7) to describe experimental observations of isolated outer hair cell bundles from the 4 kHz place of the rat cochlea[64] (Table I). The values of f_{max} required for the system to function at the operating points chosen are three times or less than the maximum force that can be generated by an individual rat hair bundle.[33]

In our description the open probability of the hair bundle's transduction channels P_o, is much more sensitive to hair bundle displacement than previous models allow and experimental measurements indicate.[33,64] However, the sharpness of P_o is underestimated and has not been measured for conditions similar to those *in vivo*.[70,85] Moreover, we choose to make the hair bundle very sensitive to displacements as we are coupling a single hair bundle to a stiff cochlear partition, rather than three as *in vivo*.

5. Outer hair cell soma

We use values for the capacitance and conductance corresponding to measurements of isolated outer hair cells from

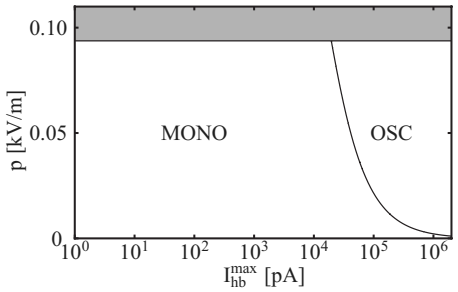

FIG. 10. State diagram for the dynamical system given in Eqs. (16)–(18) describing the active mechanics of the cochlear partition in case A, where $\gamma_1 > 0$, when the hair bundle adaptation motors are off ($f_{max}=0$). The system behavior in the absence of an external stimulus is shown as a function of the maximal current through the hair bundle I_{hb}^{max}, and the electromotility coefficient p. Spontaneous oscillations occur in the region labeled OSC and the system is monostable in the region labeled MONO. The solid line between these to regions is a line of Hopf bifurcations. A Hopf bifurcation is only possible for very large values of I_{hb}^{max}. Our description of cochlear mechanics is not valid in the shaded unphysiological region where it is necessary to take into account additional nonlinearities.

the second row of the 4 kHz region of the guinea pig cochlea.[25,28,86] The maximum current through the outer hair cell hair bundle is on the order of a few nanoamperes *in vivo*.[70,87] The value of $I_{hb}^{max}=3$ nA used in case A is well within this range. However, the value of 25 nA used in case B is less consistent with experimental data (Table II). In addition, I_{hb}^{max} is proportional to the maximum transduction channel conductance, which can vary tonotopically along the cochlea,[88] and thus it could regulate the place frequency map.

Electromotility is nonlinear over a range of about 200 mV.[29] However, the physiological range of receptor potential changes is only about 5 mV.[89] Thus, electromotility is approximately linear within the physiological range and is characterized by the linear response coefficient p. We estimate the value of the maximum electromotile response coefficient, p, from measurements of the stiffness, capacitance and the electromotile response of outer hair cells to be on the order of 10 kV/m.[25,28,86] In order to construct a system which is resonant at about 4 kHz and to take into account three outer hair cells per cochlear slice we use $p=16$ kV/m. The value of p could vary tonotopically in the cochlea. For example, p is a function of the unstimulated outer hair cell length,[90] which changes monotonically along the cochlea.[91]

APPENDIX D: ADAPTATION MOTORS OFF

Here we consider the system with the adaptation motors turned off. The remaining source of activity associated with the electrochemical gradients coupled with the nonlinearity of the hair bundle allows for spontaneous oscillations under certain conditions. The necessary conditions for oscillations are satisfied in case B when the open probability P_o of the hair bundle transduction channels is described by $\delta_{hb}=51.8$ nm and $A=2.0$. The state diagram of the system as a function of p and I_{hb}^{max} is shown in Fig. 10. Spontaneous oscillations are possible for very large values of I_{hb}^{max}. However, these values are one to two orders of magnitude larger then the physiological estimate (Table II).

[1] A. J. Hudspeth, "Making an effort to listen: Mechanical amplification in the ear," Neuron **59**, 530–545 (2008).
[2] P. Dallos, "The active cochlea," J. Neurosci. **12**, 4575–4585 (1992).
[3] G. A. Manley, "Cochlear mechanisms from a phylogenetic viewpoint," Proc. Natl. Acad. Sci. U.S.A. **97**, 11736–11743 (2000).
[4] M. A. Ruggero, N. C. Rich, A. Recio, S. S. Narayan, and L. Robles, "Basilar-membrane responses to tones at the base of the chinchilla cochlea," J. Acoust. Soc. Am. **101**, 2151–2163 (1997).
[5] L. Robles and M. A. Ruggero, "Mechanics of the mammalian cochlea," Physiol. Rev. **81**, 1305–1352 (2001).
[6] W. S. Rhode, "Observations of the vibrations of the basilar membrane using the Mössbauer technique," J. Acoust. Soc. Am. **49**, 1218–1231 (1971).
[7] P. M. Sellick, R. B. Patuzzi, and B. M. Johnstone, "Measurement of basilar membrane motion in the guinea-pig using the Mössbauer technique," J. Acoust. Soc. Am. **72**, 131–141 (1982).
[8] D. T. Kemp, "Stimulated acoustic emissions from within the human auditory system," J. Acoust. Soc. Am. **64**, 1386–1391 (1978).
[9] J. P. Wilson, "Evidence for a cochlear origin for acoustic re-emissions, threshold fine structure and tinnitus," Hear. Res. **2**, 233–252 (1980).
[10] W. S. Rhode, "An investigation of postmortem cochlear mechanics using the Mössbauer effect," *Basic Mechanisms of Hearing* (Academic, New York, 1973), pp. 49–67.
[11] M. A. Ruggero and N. C. Rich, "Application of a commercially-manufactured Doppler-shift laser velocimeter to the measurement of basilar-membrane vibration," Hear. Res. **51**, 215–230 (1991).
[12] T. Gold, "Hearing. II. the physical basis of the action of the cochlea," Proc. R. Soc., London, Ser. B **135**, 492–498 (1948).
[13] Y. Choe, M. O. Magnasco, and A. J. Hudspeth, "A model for amplification of hair-bundle motion by cyclical binding of Ca^{2+} to mechanoelectrical-transduction channels," Proc. Natl. Acad. Sci. U.S.A. **95**, 15321–15326 (1998).
[14] S. Camalet, T. Duke, F. Jülicher, and J. Prost, "Auditory sensitivity provided by self-tuned critical oscillations of hair cells," Proc. Natl. Acad. Sci. U.S.A. **97**, 3183–3188 (2000).
[15] V. M. Eguíluz, M. Ospeck, Y. Choe, A. J. Hudspeth, and M. O. Magnasco, "Essential nonlinearities in hearing," Phys. Rev. Lett. **84**, 5232–5235 (2000).
[16] P. Martin, *Active Processes and Otoacoustic Emissions* (Springer, New York, 2008), Chap. 4, pp. 93–143.
[17] R. Hallworth and H. C. Jensen-Smith, *Active Processes and Otoacoustic Emissions* (Springer, New York, 2008), Chap. 5, pp. 145–189.
[18] P. Dallos, *The Cochlea* (Springer, New York, 1996), Chap. 1, pp. 1–43.
[19] C. J. Kros, *The Cochlea* (Springer, New York, 1996), Chap. 6, pp. 318–385.
[20] M. C. Holley, *The Cochlea* (Springer, New York, 1996), Chap. 7, pp. 386–434.
[21] W. E. Brownell, C. R. Bader, D. Bertrand, and Y. De Ribaupierre, "Evoked mechanical responses of isolated cochlear outer hair cells," Science **227**, 194–196 (1985).
[22] B. Kachar, W. E. Brownell, R. Altschuler, and J. Fex, "Electrokinetic shape changes of cochlear outer hair-cells," Nature (London) **322**, 365–368 (1986).
[23] J. Ashmore, "A fast motile response in guinea-pig outer hair cells," J. Physiol. **388**, 323–347 (1987).
[24] J. Ashmore, "Cochlear outer hair cell motility," Physiol. Rev. **88**, 173–210 (2008).
[25] X. Dong, M. Ospeck, and K. H. Iwasa, "Piezoelectric reciprocal relation of the membrane motor in the cochlear outer hair cell," Biophys. J. **82**, 1254–1259 (2002).
[26] R. Patuzzi, *The Cochlea* (Springer, New York, 1996), Chap. 4, pp. 186–257.
[27] E. DeBoer, *The Cochlea* (Springer, New York, 1996), Chap. 5, pp. 258–317.
[28] S. Preyer, R. Renz, W. Hemmert, H. Zenner, and A. W. Gummer, "Receptor potential of outer hair cells isolated from base to apex of the adult guinea-pig cochlea: Implications of cochlear tuning mechanisms," Aud. Neurosci. **2**, 145–157 (1996).
[29] J. Santos-Sacchi, "On the frequency limit and phase of outer hair cell motility: Effects of the membrane filter," J. Neurosci. **12**, 1906–1916 (1992).
[30] A. C. Crawford and R. Fettiplace, "The mechanical properties of ciliary bundles of the turtle cochlear hair cells," J. Physiol. **364**, 359–379 (1985).
[31] P. Martin and A. J. Hudspeth, "Active hair-bundle movements can amplify

a hair cell's response to oscillatory mechanical stimuli," Proc. Natl. Acad. Sci. U.S.A. **96**, 14306–14311 (1999).
[32]P. Martin, D. Bozovic, Y. Choe, and A. J. Hudspeth, "Spontaneous oscillations by the hair bundles of the bullfrog's sacculus," J. Neurosci. **23**, 4533–4548 (2003).
[33]H. J. Kennedy, A. C. Crawford, and R. Fettiplace, "Force generation by the mammalian hair bundle supports a role in cochlear amplification," Nature (London) **433**, 880–883 (2005).
[34]W. Denk and W. W. Webb, "Forward and reverse transduction at the limit of sensitivity studied by correlating electrical and mechanical fluctuations in frog saccular hair cells," Hear. Res. **60**, 89–102 (1992).
[35]P. Martin and A. J. Hudspeth, "Compressive nonlinearity in the hair bundle's active response to mechanical stimulation," Proc. Natl. Acad. Sci. U.S.A. **98**, 14386–14391 (2001).
[36]D. K. Chan and A. J. Hudspeth, "Ca^{2+} current-driven nonlinear amplification by the mammalian cochlea in vitro," Nat. Neurosci. **8**, 149–155 (2005).
[37]M. C. Liberman, J. Gao, D. Z. Z. He, X. Wu, S. Jia, and J. Zuo, "Prestin is required for electromotility of the outer hair cell and for the cochlear amplifier," Nature (London) **419**, 300–304 (2002).
[38]P. Dallos, X. Wu, M. Cheatham, J. Gao, J. Zheng, C. Anderson, S. Jia, X. Wang, W. Cheng, and S. Sengupta, "Prestin-based outer hair cell motility is necessary for mammalian cochlear amplification," Neuron **58**, 333–339 (2008).
[39]G. Frank, W. Hemmert, and A. W. Gummer, "Limiting dynamics of high-frequency electromechanical transduction of outer hair cells," Proc. Natl. Acad. Sci. U.S.A. **96**, 4420–4425 (1999).
[40]G. D. Housley and J. F. Ashmore, "Ionic currents of outer hair cells isolated from the guinea-pig cochlea," J. Physiol. **448**, 73–98 (1992).
[41]E. K. Weitzel, R. Tasker, and W. E. Brownell, "Outer hair cell piezoelectricity: Frequency response enhancement and resonance behavior," J. Acoust. Soc. Am. **114**, 1462–1466 (2003).
[42]A. A. Spector, A. S. Popel, R. A. Eatock, and W. E. Brownell, "Mechanosensitive channels in the lateral wall can enhance the cochlear outer hair cell frequency response," Ann. Biomed. Eng. **33**, 991–1002 (2005).
[43]Z. Liao, S. Feng, A. S. Popel, W. E. Brownell, and A. A. Spector, "Outer hair cell active force generation in the cochlear environment," J. Acoust. Soc. Am. **122**, 2215–2225 (2007).
[44]K. Dierkes, B. Lindner, and F. Jülicher, "Enhancement of sensitivity gain and frequency tuning by coupling of active hair bundles," Proc. Natl. Acad. Sci. U.S.A. **105**, 18669–18674 (2008).
[45]J. B. Allen, "Cochlear micromechanics—A physical model of transduction," J. Acoust. Soc. Am. **68**, 1660–1670 (1980).
[46]W. F. Sewell, *The Cochlea* (Springer, New York, 1996), Chap. 9, pp. 503–533.
[47]J. Zwislocki, "Theorie der schneckenmechanik (Theory of cochlear mechanics)," Acta Oto-Laryngol., Suppl. **72**, 1–76 (1948).
[48]G. Zweig, "Basilar membrane motion," Cold Spring Harb Symp. Quant Biol. **40**, 619–633 (1976).
[49]J. Lighthill, "Energy flow in the cochlea," J. Fluid Mech. **106**, 149–213 (1981).
[50]D. O. Kim, X. M. Yang, and S. T. Neely, "An active cochlear model with negative damping in the partition: Comparison with Rhode's ante- and post-mortem observations," *Psychophysical, Physiological, and Behavioral Studies in Hearing* (Delft University Press, Delft, 1980), pp. 7–14.
[51]E. de Boer, "No sharpening? A challenge for cochlear mechanics," J. Acoust. Soc. Am. **73**, 567–573 (1983).
[52]R. Nobili and F. Mammano, "Biophysics of the cochlea II: Stationary nonlinear phenomenology," J. Acoust. Soc. Am. **99**, 2244–2255 (1996).
[53]T. K. Lu, S. Zhak, P. Dallos, and R. Sarpeshkar, "Fast cochlear amplification with slow outer hair cells," Hear. Res. **214**, 45–67 (2006).
[54]T. Reichenbach and A. J. Hudspeth, "A ratchet mechanism for amplification in low-frequency mammalian hearing," Proc. Natl. Acad. Sci. U.S.A. **107**, 4973–4978 (2010).
[55]N. B. Slepecky, *The Cochlea* (Springer, New York, 1996), Chap. 2, pp. 44–129.
[56]R. M. Edge, B. N. Evans, M. Pearce, C.-P. Richter, X. Hu, and P. Dallos, "Morphology of the unfixed cochlea," Hear. Res. **124**, 1–16 (1998).
[57]C.-P. Richter, R. Edge, D. Z. Z. He, and P. Dallos, "Development of the gerbil inner ear observed in the hemicochlea," J. Assoc. Res. Otolaryngol. **1**, 195–210 (2000).
[58]P. Dallos, "Organ of Corti kinematics," J. Assoc. Res. Otolaryngol. **4**, 416–421 (2003).
[59]H. J. Kennedy, M. G. Evans, A. C. Crawford, and R. Fettiplace, "Depolarization of cochlear outer hair cells evokes active hair bundle motion by two mechanisms," J. Neurosci. **26**, 2757–2766 (2006).
[60]D. K. Chan and A. J. Hudspeth, "Mechanical responses of the organ of Corti to acoustic and electrical stimulation in vitro," Biophys. J. **89**, 4382–4395 (2005).
[61]A. W. Gummer, W. Hemmert, and H. P. Zenner, "Resonant tectorial membrane motion in the inner ear: Its crucial role in frequency tuning," Proc. Natl. Acad. Sci. U.S.A. **93**, 8727–8732 (1996).
[62]F. Mammano and J. F. Ashmore, "Reverse transduction measured in the isolated cochlea by laser Michelson interferometry," Nature (London) **365**, 838–841 (1993).
[63]B. Nadrowski, P. Martin, and F. Jülicher, "Active hair-bundle motility harnesses noise to operate near an optimum of mechanosensitivity," Proc. Natl. Acad. Sci. U.S.A. **101**, 12195–12200 (2004).
[64]J. Tinevez, F. Jülicher, and P. Martin, "Unifying the various incarnations of active hair-bundle motility by the vertebrate hair cell," Biophys. J. **93**, 4053–4067 (2007).
[65]P. Wangemann and J. Schacht, *The Cochlea* (Springer, New York, 1996), Chap. 3, pp. 130–185.
[66]B. Hille, *Ionic Channels of Excitable Membranes*, 3rd ed. (Sinauer Associates Inc., Sunderland, 2001), Chap. 1, pp. 1–22.
[67]M. M. Mellado Lagarde, M. Drexl, A. N. Lukashkin, J. Zuo, and I. J. Russell, "Prestin's role in cochlear frequency tuning and transmission of mechanical responses to neural excitation," Curr. Biol. **18**, 200–202 (2008).
[68]F. Mammano and R. Nobili, "Biophysics of the cochlea: Linear approximation," J. Acoust. Soc. Am. **93**, 3320–3332 (1993).
[69]T. Duke and F. Jülicher, "Active traveling wave in the cochlea," Phys. Rev. Lett. **90**, 158101 (2003).
[70]H. J. Kennedy, M. G. Evans, A. C. Crawford, and R. Fettiplace, "Fast adaptation of mechanoelectrical transducer channels in mammalian cochlear hair cells," Nat. Neurosci. **6**, 832–836 (2003).
[71]W. Dong and E. S. Olson, "Middle ear forward and reverse transmission in gerbil," J. Neurophysiol. **95**, 2951–2961 (2006).
[72]I. J. Russell and A. N. Lukashkin, *Active Processes and Otoacoustic Emissions* (Springer, New York, 2008), Chap. 10, pp. 343–379.
[73]J. J. Guinan, *The Cochlea* (Springer, New York, 1996), Chap. 8, pp. 435–502.
[74]H. Goldstein, *Classical Mechanics*, 2nd ed. (Addison-Wesley, Reading, MA, 1980), Chap. 1, pp. 1–34.
[75]A. W. Gummer, B. M. Johnstone, and N. J. Armstrong, "Direct measurement of basilar membrane stiffness in the guinea pig," J. Acoust. Soc. Am. **70**, 1298–1309 (1981).
[76]C. E. Miller, "Structural implications of basilar membrane compliance measurements," J. Acoust. Soc. Am. **77**, 1465–1474 (1985).
[77]E. S. Olson and D. C. Mountain, "In vivo measurement of basilar membrane stiffness," J. Acoust. Soc. Am. **89**, 1262–1275 (1991).
[78]E. S. Olson and D. C. Mountain, "Mapping the cochlear partition's stiffness to its cellular architecture," J. Acoust. Soc. Am. **95**, 395–400 (1994).
[79]R. C. Naidu and D. C. Mountain, "Measurements of the stiffness map challenge a basic tenet of cochlear theories," Hear. Res. **124**, 124–131 (1998).
[80]G. Emadi, C.-P. Richter, and P. Dallos, "Stiffness of the gerbil basilar membrane: Radial and longitudinal variations," J. Neurophysiol. **91**, 474–488 (2003).
[81]C.-P. Richter, G. Emadi, G. Getnick, A. Quesnel, and P. Dallos, "Tectorial membrane stiffness gradients," Biophys. J. **93**, 2265–2276 (2007).
[82]B. Shoelson, E. K. Dimitriadis, H. Cai, B. Kachar, and R. S. Chadwick, "Evidence and implications of inhomogeneity in tectorial membrane elasticity," Biophys. J. **87**, 2768–2777 (2004).
[83]R. Gueta, D. Barlam, R. Z. Shneck, and I. Rousso, "Measurement of the mechanical properties of isolated tectorial membrane using atomic force microscopy," Proc. Natl. Acad. Sci. U.S.A. **103**, 14790–14795 (2006).
[84]R. Gueta, D. Barlam, R. Z. Shneck, and I. Rousso, "Sound-evoked deflections of outer hair cell stereocilia arise from tectorial membrane anisotropy," Biophys. J. **94**, 4570–4576 (2008).
[85]R. Fettiplace, "Active hair bundle movements in auditory hair cells," J. Physiol. **576**, 29–36 (2006).
[86]K. H. Iwasa and M. Adachi, "Force generation in the outer hair cell of the cochlea," Biophys. J. **73**, 546–555 (1997).
[87]D. Z. Z. He, J. Shuping, and P. Dallos, "Mechanoelectrical transduction of adult outer hair cells studied in a gerbil hemicochlea," Nature (London) **429**, 766–770 (2004).
[88]A. J. Ricci, A. C. Crawford, and R. Fettiplace, "Tonotopic variation in the

conductance of the hair cell mechanotransducer channel," Neuron **40**, 983–990 (2003).
[89]S. Preyer, W. Hemmert, M. Pfister, H. P. Zenner, and A. W. Gummer, "Frequency response of mature guinea-pig outer hair cells to stereociliary displacement," Hear. Res. **77**, 116–124 (1994).
[90]J. A. Tolomeo and C. R. Steele, "Orthotropic piezoelectric properties of the cochlear outer hair cell wall," J. Acoust. Soc. Am. **97**, 3006–3011 (1995).
[91]B. J. Dannhof, B. Roth, and V. Bruns, "Length of hair cells as a measure of frequency representation in the mammalian inner ear?," Naturwiss. **78**, 570–573 (1991).
[92]M. Beurg, M. G. Evans, C. M. Hackney, and R. Fettiplace, "A large-conductance calcium-selective mechanotransducer channel in mammalian cochlear hair cells," J. Neurosci. **26**, 10992–11000 (2006).
[93]M. P. Scherer and A. W. Gummer, "Impedance analysis of the organ of Corti with magnetically actuated probes," Biophys. J. **87**, 1378–1391 (2004).
[94]C.-P. Richter and A. Quesnel, "Stiffness properties of the reticular lamina and the tectorial membrane," *Auditory Mechanisms* (World Scientific, Singapore, 2006), pp. 70–78.